Methylome dynamic upon proteasome inhibition by the *Pseudomonas syringae* virulence factor Syringolin A

Bonnet DMV[1*], Grob S[2*], Tirot L[1] and Jullien PE[1†]

[1] Institute of Plant Sciences, University of Bern, Bern, Switzerland.

[2] Department of Plant and Microbial Biology, University of Zurich and Zurich-Basel Plant Science Center, University of Zurich, Zurich, Switzerland.

*co-first author

[†]*Corresponding author:* Pauline E. Jullien (pauline.jullien@ips.unibe.ch)

Abstract

DNA methylation is an important epigenetic mark required for proper gene expression and silencing of transposable elements. DNA methylation patterns can be modified by environmental factors such as pathogen infection, where modification of DNA methylation can be associated with plant resistance. To counter the plant defense pathways, pathogens produce effectors molecule, several of which act as proteasome inhibitors. Here we investigated the effect of proteasome inhibition by the bacterial virulence factor Syringolin A on genome-wide DNA methylation. We show that Syringolin A treatment results in an increase of DNA methylation at centromeric and pericentromeric regions of *Arabidopsis* chromosomes. We identify several CHH DMRs that are enriched in the proximity of transcriptional start sites. Syringolin A treatment does not result in significant changes in small RNA composition. However, significant changes in genome transcriptional activity can be observed, including a strong upregulation of resistance genes that are located on chromosomal arms. We hypothesize that DNA methylation changes could be linked to the upregulation of some atypical members of the *de novo* DNA methylation pathway: *AGO3*, *AGO9* and *DRM1*. Our data suggests that modification of genome-wide DNA methylation resulting from an inhibition of the proteasome by bacterial effectors could be part of a epi-genomic arms race against pathogens.

Keywords: DNA methylation, *Arabidopsis*, Syringolin A, proteasome inhibition, bacterial defense

36 Plants are sessile organism and must constantly adapt their gene expression to react
37 to constantly changing environments. Among other environmental stresses, the
38 infection of plants by pathogens, such as bacteria or fungi is a constant threat and
39 leads to significant losses in crop production. Plants have evolved several ways to
40 defend themselves against pathogens, starting from physical barriers, such as the
41 cuticula, to specific intra-cellular pathways that recognize pathogen effector
42 molecules. The effector-triggered immunity pathway (ETI) involves the specific
43 recognition of effector molecules that are secreted by the pathogen and counteract
44 the plant primary immune response (Jones and Dang, 2006).
45 Interestingly, several effector molecules produced by bacteria, viruses, and fungi were
46 found to inhibit the host proteasome machinery (Chiu et al., 2010; Dudler, 2013; Groll
47 et al., 2008; Jin et al., 2007; Marino et al., 2012; Sahana et al., 2012; Sorel et al., 2019;
48 Üstün and Börnke, 2014; Üstün et al., 2016; Verchot, 2016) and - more generally - to
49 regulate protein degradation (Langin et al., 2020). Thus, proteasome inhibition seems
50 to represent a common strategy used by plant pathogens. Additionally, host
51 proteasome inhibition has been shown to suppress systemic acquired resistance
52 (SAR) and to consequently increase plant susceptibility to bacterial pathogen (Üstün
53 et al., 2016). Beyond classical bacterial type III effector such as XopJ and HopM1
54 (Üstün et al., 2013; Üstün et al., 2016), which inhibit proteasome activity by interacting
55 with proteasome subunits, a virulence factor called Syringolin A (SylA) inhibits the
56 proteasome via an irreversible covalent binding to the proteasome catalytic subunits
57 (Groll et al., 2008). SylA is a small tri-peptide derivative, which is secreted by the
58 bacteria *Pseudomonas Syringae pv syringae* (*Pss*). Bacteria deficient for SylA
59 secretion are less virulent than their wild-type counterpart. SylA secretion is important

60 for the bacteria to overcome stomata closure and consequently gaining better leaf
61 penetration (Schellenberg et al., 2010). Similarly, SylA was also found to be important
62 for wound entry and colonization of the host via the vascular tissue (Misas-Villamil et
63 al., 2013). Interestingly, SylA was found to accumulate in the nucleus, which lead the
64 authors to suggest it could act preferentially on the nuclear proteasome (Kolodziejek
65 et al., 2011).
66 The proteasome is one of the main protein degradation machinery in eukaryotic cells.
67 Protein targeting to the proteasome relies in part to poly-ubiquitination by E3 ubiquitin
68 ligases (Sadanandom et al., 2012). Due to its central role in the cell, the proteasome
69 machinery is involved in several biological processes, such as hormonal signaling,
70 circadian clock as well as plant stress response (Sadanandom et al., 2012; Vierstra,
71 2009). Additionally, the proteasome has also been linked to the regulation of chromatin
72 and transcription (Geng et al., 2012). The proteasome's role in the regulation of
73 chromatin has not only been linked to the regulation of chromatin components, such
74 as histones and their assembly into nucleosomes, but also chromatin regulators, such
75 as histone chaperones and histone modifiers. (Bach and Hegde, 2016; H. Karimi
76 Kinyamu et al., 2008; Jeong et al., 2011; Lee et al., 2011). In addition, proteins
77 involved in DNA methylation were found to be regulated by the proteasome.
78 DNA methylation in *Arabidopsis* is characterized by the apposition of a methyl group
79 to cytosine residues. In plants, DNA methylation occurs on three distinct sequence
80 contexts: CG, CHG and CHH, where H stands for any nucleotide except cytosine.
81 Each methylation context is regulated by its own cognate pathway (Law and Jacobsen,
82 2010). CG methylation is maintained by the maintenance DNA methyltransferase
83 MET1 (METHYLTRANSFERASE 1). Despite the lack of evidence for a proteasome

84 regulation of the MET1 protein, other important proteins regulating CG methylation,
85 such as the VIM proteins are E3 ubiquitin ligases (Johnson et al., 2007; Kraft et al.,
86 2008; Woo et al., 2007), suggesting a link between ubiquitination and CG methylation.
87 The main enzyme linked to CHG methylation is the DNA methyltransferase CMT3
88 (CHROMOMETHYLASE 3) (Lindroth and Jacobsen, 2001). CMT3 itself was found to
89 be targeted for proteasomal degradation by an atypical JmjC domain protein, JMJ24,
90 which has E3 ubiquitin ligase activity (Deng et al., 2016). Recently, DRM2 (DOMAINS
91 REARRANGED METHYLASE 2), the main DNA methyltransferase involved in *de*
92 *novo* cytosine methylation at CHH sites was also found to be regulated by an E3
93 ubiquitin ligase named CFK1, leading to its targeting for degradation by the
94 proteasome (Chen et al., 2020). DNA methylation in all sequence contexts can,
95 therefore, be directly or indirectly linked to ubiquitin-dependent proteasome
96 degradation.
97 DNA methylation has previously been shown to be involved in the response against
98 bacterial and fungal pathogens (Deleris et al., 2016; Zhu et al., 2016). Indeed, mutants
99 with lower DNA methylation levels, such as *met1* were shown to display an increased
100 resistance to the bacteria *Pseudomonas* (Dowen et al., 2012), while mutant displaying
101 global DNA hypermethylation such as *ros1* were shown to be more susceptible to
102 *Pseudomonas*, *Fusarium,* and *Hyaloperonospora* infection (Le et al., 2014; López
103 Sánchez et al., 2016; Schumann et al., 2019; Yu et al., 2013). DNA *de novo*
104 methylation is known to be targeted by small RNA molecules of principally 24
105 nucleotides (nt) in size. This pathway is referred as RNA-directed DNA methylation
106 (RdDM) (Matzke and Mosher, 2014). Several members of the RdDM pathway were
107 also found to be involved in *Botrytis*, *Plectosphaerella,* and *Pseudomonas* resistance

108 (Agorio and Vera, 2007; López et al., 2011).*Pseudomonas* bacterial infection was
109 shown to affect genome-wide DNA methylation pattern (Dowen et al., 2012).
110 Additionally, DNA methylation is involved in transgenerational memory of bacterial
111 infection, a phenomenon referred as Transgenerational Acquired Resistance (TAR)
112 (Luna and Ton, 2012; Luna et al., 2012).
113 Noting the converging evidence for a role of DNA methylation during bacterial infection
114 as well as proteasome inhibition during this process, we sought to investigate the
115 effect of proteasome inhibition on global DNA methylation levels. Here we show that
116 genome-wide DNA methylation is affected by treatment with the proteasome inhibitor
117 SylA. SylA treatment results in a moderate genome hypermethylation in all sequence
118 context. This hypermethylation is mainly affecting centromeric region of *Arabidopsis*
119 chromosomes. We identified 10101 100bp DMRs of which 6304 are CHH-
120 hypermethylated DMRs. We could not identify major changes in small RNA
121 composition upon SylA treatment suggesting that small RNAs might not have a direct
122 effect on the observed DNA methylation changes. Furthermore, the *Arabidopsis*
123 transcriptome is strongly affected by SylA-mediated proteasome inhibition. We
124 propose that the induction of atypical members of the RdDM pathway such as *DRM1*,
125 *AGO9* and *AGO3* might explain the changes observed upon SylA treatment.

126 **RESULTS**

127 **Syringolin A induces moderate centromeric hypermethylation**

128 In order to investigate the effect of proteasome inhibition on the methylome of
129 *Arabidopsis*, we performed genome-wide bisulfite sequencing (GWBS) of *Arabidopsis*
130 plantlets treated with the bacterial virulence factor SylA, a known proteasome inhibitor
131 (Groll et al., 2008). Considering all three sequence contexts, we obtained DNA

132 methylation levels for 14269258 and 10867987 cytosines for mock- and sylA-treated
133 GWBS libraries, respectively, that reached more than 10-fold coverage. The obtained
134 data were plotted as a circular heat map using 50 kb genomic bins (Fig 1A). We
135 observed that the distribution of the genome-wide DNA methylation did not change
136 between treated and the control samples in all sequence context CG, CHG and CHH
137 (Fig 1A). As previously observed (Cokus et al., 2008; Lister et al., 2008; Stroud et al.,
138 2012), DNA methylation is higher in centromeric and pericentromeric regions of the
139 *Arabidopsis* genome, coinciding with increased transposon densities. As expected,
140 the percentage of DNA methylation is higher in CG context (28.36% and 29.25%),
141 then CHG context (12.05% and 13.62%) and finally at its lowest in CHH context
142 (3.16% and 3.54%) in both control and treated samples. In order to refine our
143 analyses, we focused on methylated windows (i.e., >40% methylation for CG, >20%
144 for CHG and >10% for CHH) (Fig 1B). We could observe a slight but consistent
145 increase in DNA methylation levels upon SylA treatment in all sequence contexts. In
146 order to investigate in which chromosomal environment this increase of DNA
147 methylation occurs, we plotted the percent of changes in DNA methylation across the
148 genome. We observed that, except for a few discreet loci on chromosome arms, most
149 of the increase in DNA methylation occurred in the centromeric and pericentromeric
150 regions of all *Arabidopsis* chromosomes (Fig 1C and Fig S1). We conclude that
151 proteasome inhibition by SylA treatment does not result in a global reprograming of
152 genome-wide DNA methylation but rather in a moderate hypermethylation of the
153 centromeric region.

154 **Syringolin A treatment results mainly in CHH DMRs**

155 To investigate the changes in DNA methylation on local scale, we identified
156 differentially methylated regions (DMRs) of 100 bp in size for each DNA methylation
157 context. To satisfy the criteria as a DMR, the respective 100 bp genomic bins had to
158 differ by at least 10 % between treatments and exhibiting a q-value < 0.05. We
159 identified a total of 10101 individual genomic bins satisfying DMR criteria (Fig 2A).
160 Most DMRs were in CHH context (9173) compared to CG (409) and CHG (672).
161 Additionally, they were mostly hyper DMRs (gain of DNA methylation) rather than hypo
162 DMRs (lost of DNA methylation). CHH DMRs were mostly corresponding to
163 transposable elements (TEs) (51%), UTRs (14%), promotors (14%), and intergenic
164 sequences (15%) and were rather depleted in genic sequences (2%) (Fig 2B).
165 Similarly, CG and CHG DMRs could also majorly be associated to TEs (Fig S2). The
166 overlap between the DMRs of different contexts is limited but the overlap is significant
167 (permutation-based *p*-value using 10^4 repetitions for all dual overlaps and triple
168 overlaps $< 10^{-4}$). Taking into account the frequent association of DMRs of all contexts
169 with TEs, we observed an especially pronounced overlap when regarding DMR -
170 associated TEs (Fig S3), suggesting that most significant changes in DNA methylation
171 occurs within or at proximity of TEs. In order to visualize in which genomic region
172 DMRs are located, we plotted the DMRs along the five *Arabidopsis* chromosomes (Fig
173 2C). Both hypo and hyper CHH DMRs are enriched in centromeric and pericentromeric
174 region mirroring the TE density distribution in the *Arabidopsis* genome. In order to
175 better characterize the DMRs location and their potential effect on gene expression,
176 we computed the distribution of their mean distance to transcriptional start sites (TSS)
177 and compared it to that of non-DMR methylated regions. For this purpose, we
178 separated our analysis between the DMRs occurring in the pericentromeric regions

179 and the DMRs occurring on chromosomal arms. Interestingly, SylA induced DMRs in
180 chromosomal arms are closer to TSS compared to randomly sampled methylated
181 regions for both DMRs associated with TEs (Fig 2D) and genes (Fig 2E). This
182 increased proximity to TSS is more pronounced for CHH DMRs (Fig 2D-E) than for
183 CG and CHG DMRs (Fig S4A-B). No significant differences were observed for DMRs
184 situated in pericentromeric regions (Fig S4 C-D). In summary, our results show that
185 SylA treatment results principally in CHH DMRs situated in centromeric and
186 pericentromeric region and that DMRs situated in chromosomal arms are in close
187 proximity to TSS.
188 As previously mentioned, DNA methylation changes were observed upon *Arabidopsis*
189 infection by the bacteria *Pst* (Dowen et al., 2012). In order to evaluate how similar SylA
190 DMRs are from *Pst* induced DMRs, we analyzed the overlap between *Pst* and SylA
191 DMR associated features (Fig S8A-C)). Although no significant overlap could be
192 observed for CG DMRs or CHG DMRs (Fig S8A-B), a significant overlap could be
193 observed concerning CHH DMRs with 413 overlapping loci (p-value $< 10^{-4}$) (Fig S8C).
194 The overlap between *Pst* and SylA DMRs suggests that these DMRs could be linked
195 to proteasome inhibition taking place during *Pst* infection. Further studies will be
196 required to confirm this hypothesis.

197 **Syringolin A treatment does not influence small RNA population**

198 DNA methylation in CHH context is closely link to the RNA-directed DNA methylation
199 pathway (RdDM). This pathway relies on small RNAs to induce DNA methylation at
200 the complementary DNA locus. In its canonical form, RdDM relies on the loading of
201 24nt small RNAs by AGO4 or AGO6 and the recruitment of the *de novo*
202 methyltransferase DRM2 to the DNA (Law and Jacobsen, 2010; Matzke and Mosher,

203 2014). In order to investigate potential changes in small RNA populations between
204 mock-treated and SylA-treated plantlets, we profiled the small RNA populations using
205 next-generation sequencing. As expected in both conditions, 24nt small RNAs
206 comprise the most abundant size fraction and are mostly starting with a 5'A and are
207 predominantly mapping to TEs (Fig3A-C). In both samples, the second most abundant
208 are 21nt small RNAs. They are mainly starting with a 5'T and likely correspond to
209 microRNAs. 22nt small RNA are the least abundant of the three sizes, predominantly
210 starting with a 5'G and mapping to TEs. We conclude that the overall small RNA
211 composition is very similar between the control and the treated samples and
212 comparable to previously published *Arabidopsis* small RNA compositions (Mi et al.,
213 2008). To investigate the small RNA population in more detail, we selected 100bp
214 genomic bins showing differential expression (exhibiting at least 10 reads across the
215 two treatments and showing at least a 4-fold change between the treatments). We
216 found that despite being very similar, several bins (n=1539) mostly comprising 24nt
217 small RNAs (n=1016) were enriched in the SylA-treated sample (Fig 3D). Bins
218 enriched in 21nt and 22nt small RNA were not as abundant (21 nt: 326, 22 nt: 197)
219 (Fig 3D). For all sRNA sizes we identified only a low number of sRNA depleted bins
220 (n=192). As expected, the enriched 24nt sRNAs were predominantly starting with a
221 5'A and mapping to TEs (Fig S9A-C). The enriched 21nt and 22nt small RNA had an
222 unusual 5'C and 5'T enrichment, respectively, and were predominantly mapping to
223 TEs (Fig S9A-C). In comparison to the total library populations, 21 nt sRNA,
224 presumably representing microRNAs, were underrepresented in the SylA enriched
225 sRNA population, indicating that micro RNAs are not activated upon SylA exposition.
226 Bins enriched in 24nt sRNA are located principally to pericentromeric regions (Fig S5).

227 However, only 49 of the 1055 24nt enriched bins overlapped with CHH DMR bins (Fig
228 3E, p=0.9437). The same observation was made for 21nt and 22nt enriched small
229 RNA bins (Fig S6D-F). Additionally, we could not find a significant correlation between
230 the increase in 24nt sRNAs and the CHH methylation levels (Fig 3F). The absence of
231 significant correlation was also observed for 21nt and 22nt enriched bins (Fig S6A-C).
232 We conclude that the small RNA composition is mostly unaffected by the SylA
233 treatment and that the moderate changes in sRNA composition or abundance do not
234 correlate with the changes in CHH DNA methylation and is likely not the cause of this
235 changes.

236 **Syringolin A treatment predominantly affects transcription in chromosomal**
237 **arms**

238 DNA methylation is a well-known regulator of gene and transposon expression. In
239 order to investigate a potential link between the observed changes in DNA methylation
240 upon SylA treatment and genome-wide transcriptional activity, we subjected our
241 samples to RNA sequencing. Upon SylA treatment, we could detect a major change
242 in transcriptional activity (Fig 4A-B), identifying a total of 3241 differentially expressed
243 transcripts (adjP < 0.01 and abs(logFC) > 2), among them 2945 differentially
244 expressed genes (DEG). We noted a bias toward upregulated DEGs (1675) compared
245 to downregulated DEGs (1270), showing that SylA treatment rather leads to
246 transcriptional up-regulation than down-regulation. Interestingly, gene ontology (GO)
247 term enrichment analysis for the upregulated DEGs revealed an enrichment in
248 "positive regulation of RNA polymerase II initiation" (GO:0045899, pVal= $9.4*10^{-6}$) (Fig
249 4D, Table S1). Our results suggest that an inhibition of the proteasome using SylA
250 results in an increased transcriptional activity. We can observe a similar GO term

251 enrichment in "positive regulation of RNA polymerase II initiation" (GO:0045899, pVal=
252 $2.7*10^{-9}$) using previously published transcriptomic data using MG132, a non-covalent
253 proteasome inhibitor (Table S1) (Gladman et al., 2016). This suggests that this feature
254 in not only linked to SylA itself but more generally to proteasome inhibition. Increased
255 transcriptional activity in response to proteasome inhibition seems to be widely
256 conserved, as it was also observed in human cells treated with MG132 (Kinyamu et al
257 2019).
258 As previously reported upon SylA treatment (Michel et al., 2006), we observed an
259 enrichment in "proteasome assembly" (GO:0043248, pVal= 10^{-9}). We hypothesize that
260 in order to compensate for the inhibition of the proteasome, proteasome related genes
261 are transcribed at higher levels. This phenomena was also observed using MG132
262 (Table S1) (Gladman et al., 2016). Similarly, an increase of proteasome-related gene
263 expression also occurs during *Pst* infection (Üstün et al., 2018), further supporting that
264 proteasome inhibition genuinely happen during *Pst* infection. In addition, up-regulated
265 DEGs are enriched in GO terms describing several abiotic and biotic stresses (Fig
266 4D). Down-regulated DEGs are clearly enriched in GO terms related to photosynthesis
267 as well as response to light (Fig 4C, Table S1). A link between ubiquitin-dependent
268 proteasome degradation and light response in Arabidopsis has been long established
269 with the discovery in plant of the COP9 signalosome (Chamovitz et al., 1996; Cope
270 and Deshaies, 2003; Wei and Deng, 2003).In addition to modifying gene expression,
271 SylA treatment also affects the expression of TEs, 217 of them exhibiting significantly
272 differential expression (Fig 4A-B), with a strong tendency towards being upregulated
273 rather than downregulated (up: 145, down:72). Surprisingly and similarly to DEGs, we
274 predominantly detected differentially expressed TEs located on chromosomal arms

275 rather than pericentromeric or centromeric region (Fig 4B), despite the majority of TEs
276 being located there. Upregulated TEs are enriched in LTR-copia TE families (Fig S7),
277 whereas downregulated TE tend to be enriched in DNA-MuDR transposons (Fig S7).
278 Our result shows that SylA treatment has an important effect on *Arabidopsis*
279 transcriptome, which is likely linked to role of SylA as a proteasome inhibitor.

280 **Syringolin A treatment induces the expression of atypical DNA methylation**
281 **factors**

282 In order to understand how SylA could influence DNA methylation beyond its role in
283 inhibiting the proteasome, we investigated if it could act by modulating the expression
284 of key actors of DNA methylation. We have focused our analyses on the key members
285 of the different DNA methylation pathways and homologous genes encoded in the
286 *Arabidopsis* genome (Fig 5A). Methylation on CG sites requires the principal CG DNA
287 methyltransferase *MET1* (Ennis et al., 1996; Kankel et al., 2003; Saze et al., 2003).
288 Additionally, on centromere and pericentromeric sequences, the chromatin
289 remodelers *DDM1* and *MOM1* are required for the maintenance of CG methylation
290 (Jeddeloh et al., 1998; Zemach et al., 2013). In addition, the *Arabidopsis* genome
291 encodes 3 other *MET* genes: *MET2a*, *MET2b* and *MET3* (Jullien et al., 2012). None
292 of these proteins affecting CG methylation showed a sufficient expression fold-change
293 to meet DEG criteria. Similarly, the CHG DNA methyltransferases (*CMT1*, *CMT2* and
294 *CMT3*) (Henikoff and Comai, 1998; Lindroth et al., 2001) and the DNA demethylase
295 (*ROS1*, *DME*, *DML2* and *DML3*) (Choi et al., 2002; Gong et al., 2002; Penterman et
296 al., 2007) were not among DEGs. However, we observed a significant upregulation for
297 some members of the *de novo* DNA methylation RdDM pathway, which elicits CHH
298 methylation. We analyzed the *de novo* DNA methyltransferases *DRM1*, *DRM2* and

299 *DRM3*. We could observe a significant induction of *DRM1* (log2(FC)=5.9). A significant
300 increase in transcript abundance could be observed from 8h post induction. In the
301 RdDM pathway, small RNA molecules, loaded in protein called Argonautes, are
302 targeting *de novo* methylation on the complementary DNA sequence. The Argonautes
303 associated we the RdDM pathway are *AGO4*, *AGO6*, *AGO9*, *AGO8* and *AGO3* (Duan
304 et al., 2015; Havecker et al., 2010; Huang et al., 2016; Stroud et al., 2012; Zilberman
305 et al., 2003). We found that *AGO3* (log2(FC)=3.4) and *AGO9* (log2(FC)=2.2) were
306 significantly upregulated in response to SylA treatment. Performing quantitative PCR
307 on *Arabidospis* cDNA, we could confirm that SylA treatment leads to an upregulation
308 of *AGO3*, *AGO9* and *DRM1* (Fig 5B).

309 **DISCUSSION**

310 Our study shows that Syringolin A, a virulence factor secreted by *Pseudomonas Pss*
311 strains, induces moderated change of the *Arabidopsis* methylome. Differentially
312 methylated regions are mostly located in the centromeric and pericentromeric regions
313 of the *Arabidopsis* chromosomes. Upon SylA treatment, substantial changes in the
314 *Arabidopsis* transcriptome are observed, which are most likely linked to SylA action
315 on the proteasome rather than on its effect on DNA methylation. We identified potential
316 candidate genes that could be involved in the observed increase in DNA methylation
317 levels. These candidates are atypical members of the RNA directed DNA methylation
318 pathway: *AGO3*, *AGO9* and *DRM1*.

319 Beyond SylA treatment, dynamic changes in centromeric DNA methylation seems to
320 also occur during *Arabidopsis* infection by *Pseudomonas synringae pv. tomato* (*Pst*),
321 which in contrast to *Pseudomonas synringae pv synringae* (*Pss*) does not secrete
322 SylA. Changes in DNA methylation levels during *Pseudomonas* infection were

323 previously reported (Dowen et al., 2012; Pavet et al., 2006). Pavet *et al* showed that
324 DNA methylation decreases in centromeric region during early infection (1 day post
325 infection) with *Pst* (Pavet et al., 2006), whereas Dowen *et al* report an increase of
326 centromeric DNA methylation at five days post infection. At 5 days post infection,
327 similar to SylA treated plantlets, the increase of DNA methylation was clear in the CHG
328 and less pronounced in CG and CHH context. Despite not secreting SylA, *Pst* also
329 uses type III effectors, such as HopM1, to inhibit the proteasome during infection
330 (Üstün et al., 2016). It is therefore likely that at least parts of the DNA methylation
331 changes observed during *Pst* infection, at 5 days after infection, could be linked to
332 proteasome inhibition by type III effectors as we have observed using SylA.
333 Considering the temporal effect of the infection on centromeric DNA methylation, one
334 may speculate that an early response of plants to infection triggers DNA
335 demethylation, as suggested by centromeric demethylation at 1dpi and the preferential
336 reactivation and, thus, upregulation of transposable elements (TEs) observed upon
337 Flagellin treatment (Yu et al., 2013). This DNA demethylation has been associated
338 with the expression of NBR/LRR genes which are often in close proximity to TEs. At
339 later stages of infection, however, the action of bacterial effectors, such as proteasome
340 inhibitors, might counter act this DNA demethylation and induce centromeric
341 hypermethylation.
342 Interestingly, in contrast to the changes in DNA methylation mainly occurring in
343 centromeric and pericentromeric regions, we observed the majority of differentially
344 expressed TEs and DEGs to be located on chromosomal arms. If linked, such
345 phenomena would imply a *trans* effect of the centromere DNA methylation and/or
346 organization on the expression of genes situated on the chromosomal arms. Such a

347 potential *trans* effect has been noted previously in response to *Pst* infection
348 (Cambiagno et al., 2018). Indeed, loss of centromeric and pericentromeric DNA
349 methylation in early infection has been hypothesized to be linked to the activation of
350 NBS/LRR disease resistance genes situated on chromosomal arms (Cambiagno et
351 al., 2018). It was hypothesized that centromeric hypomethylation would lead to a
352 recruitment of the RdDM RNA machinery to the centromere in order to remethylate
353 centromeric TE dense regions. As a consequence, the RdDM machinery would be
354 depleted from the chromosomal arm and would therefore facilitate PRR/NLR genes
355 expression. Another hint for a *trans* effect during infection came from epigenetic
356 quantitative trait loci (QTL) linked with increased resistance to the fungi
357 *Hyaloperonospora.* These epigenetic QTLs are located in pericentromeric regions but
358 are associated to increased priming of resistance genes situated on chromosomal
359 arms (Furci et al., 2019). It was hypothesized that this *trans*-effect might be due to
360 changes in the 3D organization of the genome that would affect genes transcriptional
361 activity. However, to date, it is still not fully clear how centromeric and pericentromeric
362 DNA methylation and/or organization would affect the expression of resistance genes
363 *in trans*. Further studies will be required to evaluate if this *trans* effect is causative or
364 just correlative and to investigate the potential molecular mechanisms of this *trans*-
365 effect.
366 Here we have shown that SylA treatment induces the expression of atypical RdDM
367 components: *DRM1*, *AGO9* and *AGO3*. *DRM1* was previously shown to be mainly
368 active during sexual reproduction (Jullien et al., 2012). Being preferentially involved in
369 CHH methylation, the significant upregulation of DRM1 may at least in part explain the
370 high abundance of CHH DMRs compared to the two other sequence contexts.

371 Interestingly, *AGO3* and *AGO9* were also characterized for their specificity to the
372 reproduction phase of the *Arabidopsis* life cycle (Jullien et al., 2020; Olmedo-Monfil et
373 al., 2010). So far, their role during bacterial infection remains to be investigated. The
374 variation in genome-wide DNA methylation pattern upon proteasome inhibition by SylA
375 could in part be linked to the up-regulation of these atypical RdDM components. Lastly,
376 it is tempting to speculate that a DNA methylation reprogramming akin to the one
377 happening during sexual reproduction might also happen during bacterial infection and
378 be part of the plant defense mechanism.
379

380 **MATERIAL AND METHODS**

381 **Plant materials and growth condition**

382 Arabidopsis thaliana Wild-type Colombia-0 (*Col-0*) one week old seedlings were used
383 throughout this study. Seeds were obtained from the NASC stock center (number
384 N22681), stratified at 4°C for 2-3 days and germinated in sterile petri dish containing
385 half Murashige and Skoog Basal Medium pH 5.7 (Ms ½, 0.8% micro agar and 0.215%
386 MS in pH5.7 miliQ H2O). Seedlings were grown in the growth chamber under long-
387 day conditions: 15 hours of light at 25°C and 60% of humidity and 10 hours of night at
388 21°C and 75% of humidity.

389 **Treatment with Syringolin A**

390 Three to five one week old plantlets were transferred in a 24 wells plate with 500µL of
391 liquid Ms ½. The plate was then return to the growth chamber and place under
392 agitation. Seedlings were allowed to recover for 24h. After recovery, the seedlings
393 were treated with Syringolin A (SylA) at a final concentration of 20µM during 24h.

394 Syringolin A stock solution (10mM in water) was stored at -20°C. After 24h hours,
395 seedlings were collected and immediately frozen in liquid nitrogen and use for
396 subsequent extraction.

397 **Sample preparation, qPCR and sequencing**

398 Total RNA was extracted from seedlings using QIAzol Lysis Reagent (Qiagen). All
399 samples were treated with DNase I (ThermoScientific) at 37°C for 30 minutes. DNAse
400 I was subsequently inactivated by addition of EDTA and heat treatment (65°C for 10
401 minutes). First-strand cDNA were synthesized using 1yg of DNase treated total RNA
402 and the Maxima First Strand cDNA Synthesis Kit (ThermoScientific), containing both
403 oligo-dT and random hexamer primers. qPCR tests were performed with a
404 QuantStudio 5 (ThermoScientific) using SYBR green (KAPA SYBR FAST qPCR
405 Master Mix). qPCR mix were prepared according to the manufacturer's protocol
406 (KAPA Biosystems). An RNA equivalent of 25 ng of cDNA templates was distributed
407 for each reaction. The qPCR program was as follow: 95 °C for 3 minutes followed by
408 45 cycles of 95 °C for 5 seconds and 60 °C for 30 seconds. ACTIN2 (AT3G18780)
409 expression was used to normalize the transcript level in each sample. For each
410 condition, RNA abundance of target genes was calculated from the average three
411 independent biological replicates with three qPCR technical replicates. Real-time PCR
412 primers used in this study are listed in Table S2.

413 For Genome wide bisulfite sequencing, seedlings genomic DNA was extracted using
414 DNeasy Plant Mini Kit and was then processed and sequenced by Novogene
415 (https://en.novogene.com/). Total sRNAs were trizol extracted and then processed
416 into sequencing libraries and sequenced by Fasteris (http://www.fasteris.com,
417 Switzerland). Total RNAs were extracted and DNAseI treated as previously

418 mentioned. mRNA libraries were prepared and sequenced by Novogene
419 (https://en.novogene.com/).

420 **Bioinformatics**

421 *mRNA profiling*

422 Paired-end raw mRNA sequencing reads from two biological replicates per treatment
423 regime were aligned to the *Arabidopsis thaliana* TAIR 10 genome assembly using
424 HISAT2 (Kim et al, 2015), using default settings but setting maximal intron length at
425 10 kb. Aligned reads have been sorted using samtools sort command (Li et al., 2009).
426 Aligned and sorted mRNA sequencing reads were mapped to genomic features using
427 featureCounts (Liao et al., 2014). Multi-mapping reads were counted by assigning
428 fractional counts to the respective features ("--fraction" option). Feature positional
429 information was provided by a custom-made SAF file containing gene (and
430 corresponding exon), transposable_element_gene, transposable_element,
431 pseudogene, miRNA, ncRNA, snoRNA, tRNA, rRNA features retrieved from TAIR 10
432 gff annotion (TAIR10_GFF3_genes_transposons.gff obtained from
433 www.arabidopsis.org). Differential expression has been analyzed using the R package
434 edgeR (Robinson et al., 2010) using the exactTest function. Features with less than
435 15 reads across all samples were omitted. Differentially expressed features were
436 defined by an absolute logFC > 2 and an adjusted *P*-value < 0.01. All plots have been
437 generated using R-base functions. Gene ontology (GO) enrichment analysis has been
438 performed using the R package topGO (Alexa et al., 2006) using GO term dataset
439 "athaliana_eg_gene" retrieved form www.plants.ensembl.org. GO enrichment has
440 been performed separately for up- and down-regulated DEGs.

441 *small RNA profiling*

442 Raw small RNA sequencing reads have been trimmed and subsequently filtered to
443 remove reads mapping two rDNA loci (Chr2:1-10000 and Chr3:14194000-14204000),
444 which have previously been repeatedly observed as a source of high number of
445 sRNAs in *Arabidopsis thaliana* seedlings and, thus, compromise later analysis.
446 Filtered sRNA reads were aligned to the Arabidopsis TAIR10 genome assembly using
447 bowtie (Langmead et al., 2009) with the following options: -a --best --strata -m 10000.
448 The aligned and sorted sRNA reads were split by size using a custom AWK script and
449 were subsequently mapped to 100 bp genomic bins using HiCdat (Schmid et al.,
450 2015). Only genomic bins, in which at least one of the samples had >= 10 reads were
451 kept for further analysis. Both Ctrl and SylA had near identical effective library sizes
452 (44810122 and 44827416 for sRNA between 17- 30 nt), thus no further normalization
453 has been performed. Genomic bins, which differed by more than 4-fold counts were
454 considered differential sRNA bins for further analysis. To assign specific genomic
455 features to differential sRNA bins, all non-ambiguous gff annotations have been
456 extended by 1 kb up- and downstream of the start and end site and sRNA bins falling
457 within these intervals were associated with the respective annotation unit. 5'
458 nucleotide identity has been assessed by a custom AWK script, taking into account all
459 aligned sRNA reads of a given length within the respective 100 bp sRNA bins, whereas
460 the sRNA read start had to lie within the bin. To associate differential sRNA bins with
461 specific feature types, we employed bedtools intersect using custom-made bed files
462 for different feature types, including promotor (defined as 1 kb upstream of TSSs of
463 gene annotations), intergenic (excluding promotors), tRNA, miRNA, pseudogenes, TE
464 (combination of transposable_element and transposable_element_gene, UTR
465 (excluding promotor), intron, CDS (gene coordinates – introns). The initial coordinates

466 for the features were retrieved from the publicly available TAIR10 gff file (see mRNA
467 profiling).

468 *Cytosine methylation analysis*

469 Illumina sequencing from bisulfite-treated genomic DNA was aligned using bismark
470 (Krueger and Andrews, 2011) with the following parameters: -q --score-min L,0,-0.2 -
471 -ignore-quals --no-mixed --no-discordant --dovetail --maxins 500. Sorted alignment
472 files were analyzed for their cytosine methylation levels employing the R package
473 methylKit (Akalin et al., 2012). Thereby, aligned reads were processed with the
474 processBismarkAln() function setting the minimal coverage at 10 and minimal quality
475 score at 20. Subsequently, methylation information per 100 bp genomic bin was
476 generated using the tileMethyCounts() function. Differentially methylated regions
477 (DMRs) were extracted using a q-value threshold of 0.05 and methylation difference
478 cutoff of 10%. For further statistical analyses, methylated regions were defined with a
479 cutoff of 40 % mC for CG context, 20 % for CHG context, and 10 % for CHH context.
480 To associate a specific genomic feature (e.g., gene identifier) with a DMR, the DMR
481 had to be positioned within a range of 1 kb 5' of the annotation start to 1kb 3' of the
482 annotation end. To associate DMRs with specific feature types, we employed bedtools
483 intersect using custom-made bed files for different feature types previously used to
484 analyze feature type distribution in differential sRNA bins.

485 Raw data are deposited on GEO under reference xxxx.

486

487 **ACKNOWLEDGMENTS**

488 We would like to thank the following people for their help: Jasmine Sekulovski for
489 support concerning plant growth, Gregory Schott and Olivier Voinnet for technical and

490 financial support at the early stage of this study, Robert Dudler and Zsuzsanna
491 Hasenkamp for providing Syringolin A.

492 **AUTHOR CONTRIBUTIONS**

493 PEJ conceived the study. DMVB, LT and PEJ performed the experiments. SG
494 performed the bioinformatic analysis. SG and PEJ analyzed the data. PEJ wrote the
495 manuscript with the help of SG.

496

497

498 **LITERATURE CITED**

499 **Agorio, A. and Vera, P.** (2007). ARGONAUTE4 is required for resistance to
500 Pseudomonas syringae in Arabidopsis. *Plant Cell* **19**, 3778–3790.

501 **Akalin, A., Kormaksson, M., Li, S., Garrett-Bakelman, F. E., Figueroa, M. E.,**
502 **Melnick, A. and Mason, C. E.** (2012). MethylKit: a comprehensive R package for
503 the analysis of genome-wide DNA methylation profiles. *Genome Biol.* **13**,.

504 **Alexa, A., Rahnenführer, J. and Lengauer, T.** (2006). Improved scoring of functional
505 groups from gene expression data by decorrelating GO graph structure.
506 *Bioinformatics* **22**, 1600–1607.

507 **Bach, S. V. and Hegde, A. N.** (2016). The proteasome and epigenetics: Zooming in
508 on histone modifications. *Biomol. Concepts* **7**, 215–227.

509 **Cambiagno, D. A., Nota, F., Zavallo, D., Rius, S., Casati, P., Asurmendi, S. and**
510 **Alvarez, M. E.** (2018). Immune receptor genes and pericentromeric transposons
511 as targets of common epigenetic regulatory elements. *Plant J.* **96**, 1178–1190.

512 **Chamovitz, D. A., Wei, N., Osterlund, M. T., Von Arnim, A. G., Staub, J. M., Matsui,**
513 **M. and Deng, X. W.** (1996). The COP9 complex, a novel multisubunit nuclear
514 regulator involved in light control of a plant developmental switch. *Cell* **86**, 115–
515 121.

516 **Chen, J., Liu, J., Jiang, J., Qian, S., Song, J., Kabara, R., Delo, I., Serino, G., Liu,**
517 **F., Hua, Z., et al.** (2020). F-box protein CFK1 interacts with and degrades de
518 novo DNA methyltransferase in Arabidopsis . *New Phytol.* **4**,.

519 **Chiu, M., Chen, I., Baulcombe, D. C. and Tsai, C.** (2010). The silencing suppressor
520 P25 of Potato virus X interacts with Argonaute1 and mediates its degradation
521 through the proteasome pathway. *Mol. Plant Pathol.* **11**, 641–649.

522 **Choi, Y., Gehring, M., Johnson, L., Hannon, M., Harada, J. J., Goldberg, R. B.,**
523 **Jacobsen, S. E. and Fischer, R. L.** (2002). DEMETER, a DNA glycosylase
524 domain protein, is required for endosperm gene imprinting and seed viability in
525 arabidopsis. *Cell* **110**, 33–42.
526 **Cokus, S. J., Feng, S., Zhang, X., Chen, Z., Merriman, B., Haudenschild, C. D.,**
527 **Pradhan, S., Nelson, S. F., Pellegrini, M. and Jacobsen, S. E.** (2008). Shotgun
528 bisulphite sequencing of the Arabidopsis genome reveals DNA methylation
529 patterning. *Nature* **452**, 215–219.
530 **Cope, G. A. and Deshaies, R. J.** (2003). COP9 signalosome: A multifunctional
531 regulator of SCF and other cullin-based ubiquitin ligases. *Cell* **114**, 663–671.
532 **Deleris, A., Halter, T. and Navarro, L.** (2016). DNA Methylation and Demethylation
533 in Plant Immunity. *Annu. Rev. Phytopathol.* **54**, 579–603.
534 **Deng, S., Jang, I. C., Su, L., Xu, J. and Chua, N. H.** (2016). JMJ24 targets
535 CHROMOMETHYLASE3 for proteasomal degradation in arabidopsis. *Genes*
536 *Dev.* **30**, 251–256.
537 **Dowen, R. H., Pelizzola, M., Schmitz, R. J., Lister, R., Dowen, J. M., Nery, J. R.,**
538 **Dixon, J. E. and Ecker, J. R.** (2012). Widespread dynamic DNA methylation in
539 response to biotic stress. *Proc. Natl. Acad. Sci.* **109**, E2183–E2191.
540 **Duan, C., Zhang, H., Tang, K., Zhu, X., Qian, W., Hou, Y., Wang, B., Lang, Z., Zhao,**
541 **Y., Wang, X., et al.** (2015). Specific but interdependent functions for A rabidopsis
542 AGO 4 and AGO 6 in RNA -directed DNA methylation . *EMBO J.* **34**, 581–592.
543 **Dudler, R.** (2013). Manipulation of host proteasomes as a virulence mechanism of
544 plant pathogens. *Annu. Rev. Phytopathol.* **51**, 521–42.
545 **Ennis, E. L. S. D., Finnegan, E. J., Peacock, W. J. and Dennis, E. S.** (1996).

546 Reduced DNA methylation in Arabidopsis thaliana results in abnormal plant
547 development. *Proc. Natl. Acad. Sci. U. S. A.* **93**, 8449–54.
548 **Furci, L., Jain, R., Stassen, J., Berkowitz, O., Whelan, J., Roquis, D., Baillet, V.,**
549 **Colot, V., Johannes, F. and Ton, J.** (2019). Identification and characterisation
550 of hypomethylated DNA loci controlling quantitative resistance in Arabidopsis. 1–
551 23.
552 **Geng, F., Wenzel, S. and Tansey, W. P.** (2012). Ubiquitin and Proteasomes in
553 Transcription. *Annu Rev Biochem* **81**, 177–201.
554 **Gladman, N. P., Marshall, R. S., Lee, K. H. and Vierstra, R. D.** (2016). The
555 proteasome stress regulon is controlled by a pair of NAC transcription factors in
556 arabidopsis. *Plant Cell* **28**, 1279–1296.
557 **Gong, Z., Morales-Ruiz, T., Ariza, R. R., Roldán-Arjona, T., David, L. and Zhu, J.**
558 **K.** (2002). ROS1, a repressor of transcriptional gene silencing in Arabidopsis,
559 encodes a DNA glycosylase/lyase. *Cell* **111**, 803–814.
560 **Groll, M., Schellenberg, B., Bachmann, A. S., Archer, C. R., Huber, R., Powell, T.**
561 **K., Lindow, S., Kaiser, M. and Dudler, R.** (2008). A plant pathogen virulence
562 factor inhibits the eukaryotic proteasome by a novel mechanism. *Nature* **452**,
563 755–758.
564 **H. Karimi Kinyamu, Jefferson, W. N. and Archer, T. K.** (2008). Intersection of
565 Nuclear Receptors and the Proteasome on the Epigenetic Landscape. *Env. Mol*
566 *Mutagen* **49**, 83–95.
567 **Havecker, E. R., Wallbridge, L. M., Hardcastle, T. J., Bush, M. S., Kelly, K. A.,**
568 **Dunn, R. M., Schwach, F., Doonan, J. H. and Baulcombe, D. C.** (2010). The
569 Arabidopsis RNA-directed DNA methylation argonautes functionally diverge

570 based on their expression and interaction with target loci. *Plant Cell* **22**, 321–34.

571 **Henikoff, S. and Comai, L.** (1998). A DNA Methyltransferase Homolog With a
572 Chromodomain Exists in Multiple Polymorphic Forms in Arabidopsis. *Genetics*
573 **149**, 307–318.

574 **Huang, J., Yang, M., Lu, L. and Zhang, X.** (2016). Diverse functions of small RNAs
575 in different plant-pathogen communications. *Front. Microbiol.* **7**, 1–17.

576 **Jeddeloh, J. a., Bender, J. and Richards, E. J.** (1998). The DNA methylation locus
577 DDM1 is required for maintenance of gene silencing in Arabidopsis. *Genes Dev.*
578 **12**, 1714–1725.

579 **Jeong, C. W., Roh, H., Dang, T. V., Choi, Y. Do, Fischer, R. L., Lee, J. S. and Choi,**
580 **Y.** (2011). An E3 ligase complex regulates SET-domain polycomb group protein
581 activity in Arabidopsis thaliana. *Proc. Natl. Acad. Sci. U. S. A.* **108**, 8036–8041.

582 **Jin, Y., Ma, D., Dong, J., Jin, J., Li, D., Deng, C. and Wang, T.** (2007). HC-Pro
583 Protein of Potato Virus Y Can Interact with Three Arabidopsis 20S Proteasome
584 Subunits In Planta. *J. Virol.* **81**, 12881–12888.

585 **Johnson, L. M., Bostick, M., Zhang, X., Kraft, E., Henderson, I., Callis, J. and**
586 **Jacobsen, S. E.** (2007). The SRA Methyl-Cytosine-Binding Domain Links DNA
587 and Histone Methylation. *Curr. Biol.* **17**, 379–384.

588 **Jones, J. D. G. and Dang, J. L.** (2006). The plant immune system. *Nature* **444**, 323–
589 329.

590 **Jullien, P. E., Susaki, D., Yelagandula, R., Higashiyama, T. and Berger, F.** (2012).
591 DNA methylation dynamics during sexual reproduction in Arabidopsis thaliana.
592 *Curr. Biol.* **22**, 1825–1830.

593 **Jullien, P. E., Grob, S., Marchais, A., Pumplin, N., Chevalier, C., Bonnet, D. M. .,**

594 **Otto, C., Schott, G. and Voinnet, O.** (2020). Functional characterization of
595 Arabidopsis ARGONAUTE 3 in reproductive tissue. *Plant J.* 1796–1809.
596 **Kankel, M. W., Ramsey, D. E., Stokes, T. L., Flowers, S. K., Haag, J. R., Jeddeloh,**
597 **J. a, Riddle, N. C., Verbsky, M. L. and Richards, E. J.** (2003). Arabidopsis MET1
598 cytosine methyltransferase mutants. *Genetics* **163**, 1109–22.
599 **Kolodziejek, I., Misas-Villamil, J. C., Kaschani, F., Clerc, J., Gu, C., Krahn, D.,**
600 **Niessen, S., Verdoes, M., Willems, L. I., Overkleeft, H. S., et al.** (2011).
601 Proteasome activity imaging and profiling characterizes bacterial effector
602 Syringolin A. *Plant Physiol.* **155**, 477–489.
603 **Kraft, E., Bostick, M., Jacobsen, S. E. and Callis, J.** (2008). ORTH / VIM proteins
604 that regulate DNA methylation are functional ubiquitin E3 ligases. *Plant J.* **2**, 1–
605 12.
606 **Krueger, F. and Andrews, S. R.** (2011). Bismark: A flexible aligner and methylation
607 caller for Bisulfite-Seq applications. *Bioinformatics* **27**, 1571–1572.
608 **Langin, G., Gouguet, P. and Üstün, S.** (2020). Microbial Effector Proteins – A
609 Journey through the Proteolytic Landscape. *Trends Microbiol.* **28**, 523–535.
610 **Langmead, B., Trapnell, C., Pop, M. and Salzberg, S. L.** (2009). Ultrafast and
611 memory-efficient alignment of short DNA sequences to the human genome.
612 *Genome Biol.* **10**,.
613 **Law, J. A. and Jacobsen, S. E.** (2010). Establishing , maintaining and modifying DNA
614 methylation patterns in plants and animals. *Nat. Rev. Genet.* **11**, 204–220.
615 **Le, T. N., Schumann, U., Smith, N. A., Tiwari, S., Khang Au, P. C., Zhu, Q. H.,**
616 **Taylor, J. M., Kazan, K., Llewellyn, D. J., Zhang, R., et al.** (2014). DNA
617 demethylases target promoter transposable elements to positively regulate stress

618 responsive genes in Arabidopsis. *Genome Biol.* **15**, 1–18.

619 **Lee, K. H., Minami, A., Marshall, R. S., Book, A. J., Farmer, L. M., Walker, J. M.**
620 **and Vierstra, R. D.** (2011). The RPT2 subunit of the 26S proteasome directs
621 complex assembly, histone dynamics, and gametophyte and sporophyte
622 development in arabidopsis. *Plant Cell* **23**, 4298–4317.

623 **Li, H., Handsaker, B., Wysoker, A., Fennell, T., Ruan, J., Homer, N., Marth, G.,**
624 **Abecasis, G. and Durbin, R.** (2009). The Sequence Alignment/Map format and
625 SAMtools. *Bioinformatics* **25**, 2078–2079.

626 **Liao, Y., Smyth, G. K. and Shi, W.** (2014). FeatureCounts: An efficient general
627 purpose program for assigning sequence reads to genomic features.
628 *Bioinformatics* **30**, 923–930.

629 **Lindroth, A. M. and Jacobsen, S. E.** (2001). Requirement of
630 CHROMOMETHYLASE3 for Maintenance of CpXpG Methylation. *Science (80-.*
631 *).* **292**, 2077.

632 **Lindroth, a M., Cao, X., Jackson, J. P., Zilberman, D., McCallum, C. M., Henikoff,**
633 **S. and Jacobsen, S. E.** (2001). Requirement of CHROMOMETHYLASE3 for
634 maintenance of CpXpG methylation. *Science* **292**, 2077–80.

635 **Lister, R., O'Malley, R. C., Tonti-Filippini, J., Gregory, B. D., Berry, C. C., Millar,**
636 **A. H., Ecker, J. R., Malley, R. C. O. and Harvey, A.** (2008). Highly integrated
637 single-base resolution maps of the epigenome in Arabidopsis. *Cell* **133**, 523–36.

638 **López, A., Ramírez, V., García-Andrade, J., Flors, V. and Vera, P.** (2011). The RNA
639 silencing enzyme RNA polymerase V is required for plant immunity. *PLoS Genet.*
640 **7**,.

641 **López Sánchez, A., Stassen, J. H. M., Furci, L., Smith, L. M. and Ton, J.** (2016).

642 The role of DNA (de)methylation in immune responsiveness of Arabidopsis. *Plant*
643 *J.* **88**, 361–374.
644 **Luna, E. and Ton, J.** (2012). The epigenetic machinery controlling transgenerational
645 systemic acquired resistance. *Plant Signal. Behav.* **7**, 615–618.
646 **Luna, E., Bruce, T. J. A., Roberts, M. R., Flors, V. and Ton, J.** (2012). Next-
647 generation systemic acquired resistance. *Plant Physiol.* **158**, 844–853.
648 **Marino, D., Peeters, N. and Rivas, S.** (2012). Ubiquitination during plant immune
649 signaling. *Plant Physiol.* **160**, 15–27.
650 **Matzke, M. A. and Mosher, R. A.** (2014). RNA-directed DNA methylation: An
651 epigenetic pathway of increasing complexity. *Nat. Rev. Genet.* **15**, 394–408.
652 **Mi, S., Cai, T., Hu, Y., Chen, Y., Hodges, E., Ni, F., Wu, L., Li, S., Zhou, H., Long,**
653 **C., et al.** (2008). Sorting of small RNAs into Arabidopsis argonaute complexes is
654 directed by the 5' terminal nucleotide. *Cell* **133**, 116–27.
655 **Michel, K., Abderhalden, O., Bruggmann, R. and Dudler, R.** (2006). Transcriptional
656 changes in powdery mildew infected wheat and Arabidopsis leaves undergoing
657 syringolin-triggered hypersensitive cell death at infection sites. *Plant Mol. Biol.* **62**,
658 561–78.
659 **Misas-Villamil, J. C., Kolodziejek, I., Crabill, E., Kaschani, F., Niessen, S., Shindo,**
660 **T., Kaiser, M., Alfano, J. R. and van der Hoorn, R. A. L.** (2013). Pseudomonas
661 syringae pv. syringae Uses Proteasome Inhibitor Syringolin A to Colonize from
662 Wound Infection Sites. *PLoS Pathog.* **9**, 10–16.
663 **Olmedo-Monfil, V., Durán-Figueroa, N., Arteaga-Vázquez, M., Demesa-Arévalo,**
664 **E., Autran, D., Grimanelli, D., Slotkin, R. K., Martienssen, R. A. and Vielle-**
665 **Calzada, J.-P.** (2010). Control of female gamete formation by a small RNA

666 pathway in Arabidopsis. *Nature* **464**, 628–632.

667 **Pavet, V., Quintero, C., Cecchini, N. M., Rosa, A. L. and Alvarez, M. E.** (2006).
668 Arabidopsis displays centromeric DNA hypomethylation and cytological
669 alterations of heterochromatin upon attack by Pseudomonas syringae. *Mol. Plant-*
670 *Microbe Interact.* **19**, 577–587.

671 **Penterman, J., Zilberman, D., Huh, J. H., Ballinger, T., Henikoff, S. and Fischer,**
672 **R. L.** (2007). DNA demethylation in the Arabidopsis genome. *Proc. Natl. Acad.*
673 *Sci. USA* **104**, 6752–6757.

674 **Robinson, M. D., McCarthy, D. J. and Smyth, G. K.** (2010). edgeR: a Bioconductor
675 package for differential expression analysis of digital gene expression data.
676 *Bioinformatics* **26**, 139–140.

677 **Sadanandom, A., Bailey, M., Ewan, R., Lee, J. and Nelis, S.** (2012). The ubiquitin-
678 proteasome system: Central modifier of plant signalling. *New Phytol.* **196**, 13–28.

679 **Sahana, N., Kaur, H., Basavaraj, Tena, F., Jain, R. K., Palukaitis, P., Canto, T. and**
680 **Praveen, S.** (2012). Inhibition of the Host Proteasome Facilitates Papaya
681 Ringspot Virus Accumulation and Proteosomal Catalytic Activity Is Modulated by
682 Viral Factor HcPro. *PLoS One* **7**,.

683 **Saze, H., Mittelsten Scheid, O. and Paszkowski, J.** (2003). Maintenance of CpG
684 methylation is essential for epigenetic inheritance during plant gametogenesis.
685 *Nat. Genet.* **34**, 65–69.

686 **Schellenberg, B., Ramel, C. and Dudler, R.** (2010). Pseudomonas syringae
687 virulence factor syringolin A counteracts stomatal immunity by proteasome
688 inhibition. *Mol. Plant. Microbe. Interact.* **23**, 1287–93.

689 **Schmid, M. W., Grob, S. and Grossniklaus, U.** (2015). HiCdat: A fast and easy-to-

690 use Hi-C data analysis tool. *BMC Bioinformatics* **16**, 1–6.

691 **Schumann, U., Lee, J. M., Smith, N. A., Zhong, C., Zhu, J. K., Dennis, E. S., Millar,**
692 **A. A. and Wang, M. B.** (2019). DEMETER plays a role in DNA demethylation and
693 disease response in somatic tissues of Arabidopsis. *Epigenetics* **14**, 1074–1087.

694 **Sorel, M., Mooney, B., Marchi, R. and Graciet, E.** (2019). *Ubiquitin/Proteasome*
695 *System in Plant Pathogen Responses*.

696 **Stroud, H., Greenberg, M. V. C., Feng, S., Bernatavichute, Y. V. and Jacobsen, S.**
697 **E.** (2012). Resource Comprehensive Analysis of Silencing Mutants Reveals
698 Complex Regulation of the Arabidopsis Methylome. *Cell* **152**, 352–364.

699 **Üstün, S. and Börnke, F.** (2014). Interactions of Xanthomonas type-III effector
700 proteins with the plant ubiquitin and ubiquitin-like pathways. *Front. Plant Sci.* **5**,
701 3389.

702 **Üstün, S., Bartetzko, V. and Börnke, F.** (2013). The Xanthomonas campestris Type
703 III Effector XopJ Targets the Host Cell Proteasome to Suppress Salicylic-Acid
704 Mediated Plant Defence. *PLoS Pathog.* **9**,.

705 **Üstün, S., Sheikh, A., Gimenez-Ibanez, S., Jones, A., Ntoukakis, V. and Börnke,**
706 **F.** (2016). The proteasome acts as a hub for plant immunity and is targeted by
707 pseudomonas type III effectors. *Plant Physiol.* **172**, 1941–1958.

708 **Üstün, S., Hafrén, A., Liu, Q., Marshall, R. S., Minina, E. A., Bozhkov, P. V.,**
709 **Vierstra, R. D. and Hofius, D.** (2018). Bacteria exploit autophagy for proteasome
710 degradation and enhanced virulence in plants. *Plant Cell* **30**, 668–685.

711 **Verchot, J.-M.** (2016). Plant Virus Infection and the Ubiquitin Proteasome Machinery:
712 Arms Race along the Endoplasmic Reticulum. *Viruses* **8**, 314.

713 **Vierstra, R. D.** (2009). The ubiquitin-26S proteasome system at the nexus of plant

714 biology. *Nat. Rev. Mol. Cell Biol.* **10**, 385–397.

715 **Wei, N. and Deng, X. W.** (2003). The COP9 signalosome. *Annu. Rev. Cell Dev. Biol.*
716 **19**, 261–86.

717 **Woo, H. R., Pontes, O., Pikaard, C. S. and Richards, E. J.** (2007). VIM1, a
718 methylcytosine-binding protein required for centromeric heterochromatinization.
719 *Genes Dev.* **21**, 267–277.

720 **Yu, A., Lepère, G., Jay, F., Wang, J., Bapaume, L., Wang, Y., Abraham, A.-L.,**
721 **Penterman, J., Fischer, R. L., Voinnet, O., et al.** (2013). Dynamics and
722 biological relevance of DNA demethylation in *Arabidopsis* antibacterial defense.
723 *Proc. Natl. Acad. Sci. U. S. A.* **110**, 2389–94.

724 **Zemach, A., Kim, M. Y., Hsieh, P.-H., Coleman-Derr, D., Eshed-Williams, L., Thao,**
725 **K., Harmer, S. L. and Zilberman, D.** (2013). The Arabidopsis Nucleosome
726 Remodeler DDM1 Allows DNA Methyltransferases to Access H1-Containing
727 Heterochromatin. *Cell* **153**, 193–205.

728 **Zhu, Q. H., Shan, W. X., Ayliffe, M. A. and Wang, M. B.** (2016). Epigenetic
729 mechanisms: An emerging player in plant-microbe interactions. *Mol. Plant-*
730 *Microbe Interact.* **29**, 187–196.

731 **Zilberman, D., Cao, X. and Jacobsen, S. E.** (2003). ARGONAUTE4 control of locus-
732 specific siRNA accumulation and DNA and histone methylation. *Science* **299**,
733 716–9.

734

735

736 **Figure captions**

737 **Fig.1 Methylation changes upon Syringolin A treatment.** A) Circos plot for cytosine
738 methylation levels in CG, CHG, and CHH contexts in mock treated (Ctrl) and Syringolin
739 A treated (SylA) plantlets. Red barplots depict transposable element densities within
740 50 kb genomic bins. B) Boxplot showing global cytosine methylation levels using 100
741 bp bins. Methylated bins were defined by a minimal methylation level of 40 % for CG
742 context (Red), 20 % for CHG context (Green), and 10 % for CHH context (Blue),
743 respectively. Lighter colour represent the SylA treated sample. C) Percent methylation
744 changes along chromosome 1 for CG (red), CHG (green), and CHH (blue) context,
745 respectively (See also Fig.S1). Bottom track depicts transposable element (black) and
746 gene (grey) density in 50 kb bins as a proxy for the occurrence of heterochromatin and
747 euchromatin. Grey rectangle: pericentromere.

748 **Fig.2 DMRs induced by SylA treatment.** A) Number of hyper and hypo DMRs per
749 context. B) Pie chart representing genomic features, associated with CHH DMRs
750 (taking 1 kb 5' of the annotation start and 3' of the end position, respectively). Left:
751 CHH hyper DMRs, right: CHH hypo DMRs. Genomic features not visible on the pie
752 chart due to low occurrence of DMRs have been omitted. C) Genomic localization of
753 DMRs. The colour code indicates the number of DMRs per 50 kb genomic bin.
754 Transposable element (TE) (black) and gene density per 100 kb bin are depicted as a
755 proxy for the occurrence of heterochromatin and euchromatin, respectively. D)
756 Metaplot showing the mean distance from CHH DMRs to the putative transcriptional
757 start site (TSS) of TEs located on chromosome arms in closest proximity to the DMR.
758 DMRs within 5 kb of TEs' annotation start sites were selected. Magenta: DMRs, green:
759 randomly selected non-differentially methylated regions occurring within 5 kb of TEs'

760 annotation start sites. E) Metaplot showing the mean distance from CHH DMRs to the
761 TSS of genes located on chromosome arms in closest proximity to the DMR. DMRs
762 within 5 kb of genes located on chromosome arms were selected. Magenta: DMRs,
763 green: randomly selected non-differentially methylated regions occurring within 5 kb
764 of TSSs.

765 **Fig.3 small RNA population upon Syringolin A treatment.** A) Pie charts
766 representing sRNA size distribution (21 nt, 22 nt, 24 nt) in total mock (Ctrl) treated
767 libraries and Syringolin A (SylA) treated libraries. B) Stacked bar charts showing the
768 percentage of the 5' nucleotide identity by sRNA sizes. C) Genomic features
769 associated with sRNAs per size (21 nt, 22 nt, 24 nt). small RNA bins lying within 1 kb
770 5' of the annotation start site and 1 kb 3' of the annotation end site were selected. D)
771 Barplot featuring the number of enriched and depleted 100 bp small RNA bins upon
772 SylA treatment. E) Venn diagram showing the overlap between CHH 100 bp DMRs
773 and enriched/depleted 24 nt 100 bp sRNA bins. F) correlation analysis between
774 methylation levels of DMRs with 24nt enriched Bins showing a lack of correlation.

775 **Fig4. High number of up-regulated genes upon Syringolin A treatment.** A)
776 Volcano plot depicting up- and down-regulated genes (blue), TEs (red), and
777 pseudogenes (grey). Brown horizontal and vertical lines mark the thresholds to call
778 significantly differential expression (logFC > 2, adjusted *P*-value < 0.01). B)
779 Chromosomal location of significantly up-regulated genes (blue triangles) and TEs
780 (green triangles) and down-regulated genes (red triangles) and TEs (orange triangles).
781 Gene and TE density in 50 kb bins are shown as a proxy for the occurrence of
782 euchromatin and heterochromatin. (C-D) GO term analysis for down-regulated (C) and
783 up-regulated genes (D). Most significant 15 GO terms are shown. Bubble size

784 indicates the percentage of all down-regulated genes within the respective GO term.
785 Colour code illustrates the percentage of significant genes of all genes of the given
786 term. Complete GO Term enrichment list can be found in Table S1.

787 **Fig5. Syringolin A regulate the expression of AGO3, AGO9 and DRM1**. A)
788 Histogram showing the log Fold change of *Arabidopsis* genes involved in the DNA
789 methylation pathway. The bars are colored according to the FDR value (Red:
790 FDR<0.0001, dark blue: FDR[0.001-0.0001], light blue: FDR[0.01-0.001] and white:
791 FDR>0.01). B) Quantitative PCR showing the upregulation of *AGO3*, *AGO9* and
792 *DRM1* during a time course following a treatment of seedlings with SylA or H2O as
793 control. Individual points represent biological replicates, line represent the Mean RQ
794 value. ACT2 was used as normalizer.

Figure captions e-Xtras

Fig. S1 Percent methylation changes along chromosomes. Mean methylation change (in %) in 50 kb genomic bins, discerned by methylation context and *Arabidopsis* chromosomes 1-5. Red: hypermethylation, blue: hypomethylation. Gene (grey) and TE (yellow) densities in 50 kb are shown to highlight the occurrence of pericentromeres and chromosome arms, respectively.

Fig. S2 Genomic features associated to DMRs. Pie charts show the relative abundance of annotation feature types associated to a given type of DMR. Left: hypermethylated DMRs, right: hypomethylated DMRs, top: DMRs in CG context, middle: DMRs in CHH context, bottom: DMRs in CHG context.

Fig. S3 Overlaps between DMRs of different sequence contexts. (A-C) Venn diagrams showing overlap among the three sequence contexts (CHG, CHH, CG). A) Overlap among 100 bp genomic bins. B) Overlap among DMR-associated genes (associated with DMR, when DMR lies within – 1kb of the annotation start to +1 kb of the annotation end site) C) Overlap among DMR-associated TEs (associated with DMR, when DMR lies within – 1kb of the annotation start to +1 kb of the annotation end site).

Fig. S4 DMRs distance to transcription start site. (A-D) Metaplots representing the distribution of mean distance of DMRs to transcriptional start sites (TSSs). TSS closest to DMRs that lie within +/-5 kb of a TSS were selected. Red line: density of mean distance of DMRs to TSSs. Blue line: density of mean distance of randomly selected methylated regions (not being DMRs) that lie within +/- 5 kb of a TSS. A) TSS of TEs located on chromosome arms. B) TSS of genes located on chromosome arms. C) TSS

24 of TEs located in pericentromeric region. D) TSS of genes located in pericentromeric
25 region.

26 **Fig. S5 Genomic location of the differentially expressed sRNA bins.**
27 Chromosomal plot showing the number of differentially expressed sRNA bins along
28 the five *Arabidopsis* chromosomes. The color code refers to the number of
29 differentially expressed 100 bp sRNA bins within 50 kb genomic regions.

30 **Fig. S6 Relationship between differentially expressed sRNA bins and DNA**
31 **methylation changes.** (A-C) Scatterplots to visualize correlation analysis between
32 differentially expressed sRNA bins and CHH methylation changes within these bins.
33 A) 21nt sRNAs B) 22nt sRNAs C) 24nt sRNA. Test statistics: pearson correlation
34 analyses. (D-F) Venn diagrams showing the overlap of 100bp CHH DMRs and
35 differentially expressed 100bp sRNA bins. D) 21nt sRNA E) 22nt sRNA F) 24nt sRNA.

36 **Fig. S7 Differentially expressed TE families.** Pie charts showing the relative
37 abundance of TE families. A) Distribution of TE families in the *Arabidopsis thaliana*
38 genome (TAIR10). B) Composition of TE families in significantly up-regulated TEs
39 upon SylA treatment. C) Composition of TE families in significantly down-regulated
40 TEs upon SylA treatment.

41 **Fig. S8 Overlap between SylA and *Pst* induced DMRs.** Venn diagram representing
42 overlapping DMR associated loci in SylA (this study) and *Pst* from the study by (Dowen
43 *et al.* 2012) A) CG DMRs B) CHG DMRs C) CHH DMRs.

44 **Fig. S9. Characteristic of small RNA enriched population upon Syringolin A**
45 **treatment.** A) Pie charts representing sRNA size distribution (21 nt, 22 nt, 24 nt) in
46 total mock (Ctrl) treated libraries and Syringolin A (SylA) treated libraries, and SylA
47 enriched (logFC > 2) sRNA populations. B) Stacked bar charts showing the

48 percentage of the 5' nucleotide identity by sRNA sizes. C) Genomic features
49 associated with sRNAs per size (21 nt, 22 nt, 24 nt). small RNA bins lying within 1 kb
50 5' of the annotation start site and 1 kb 3' of the annotation end site were selected.
51
52

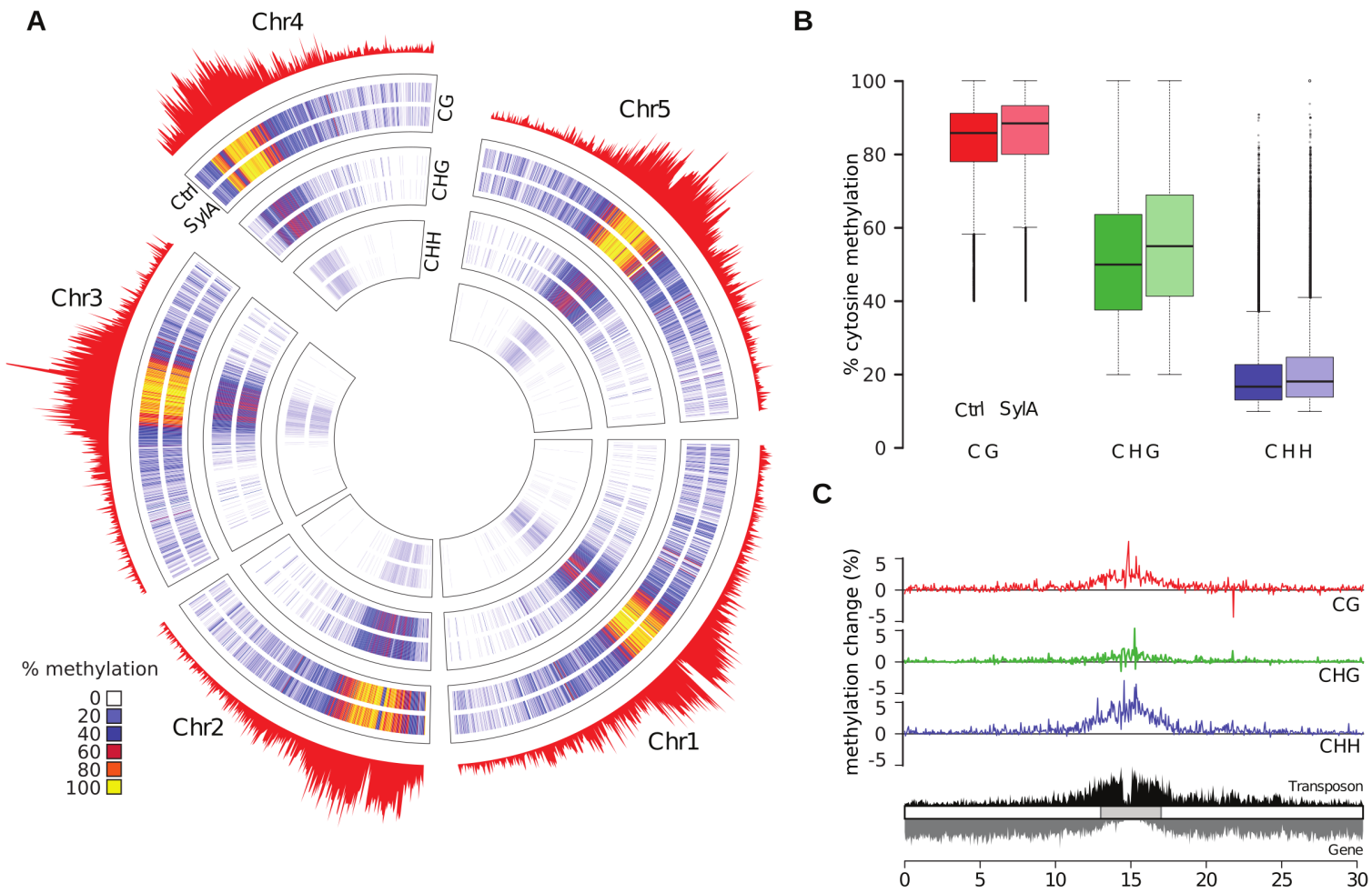

Figure 1
Methylome changes upon Syringolin A treatment

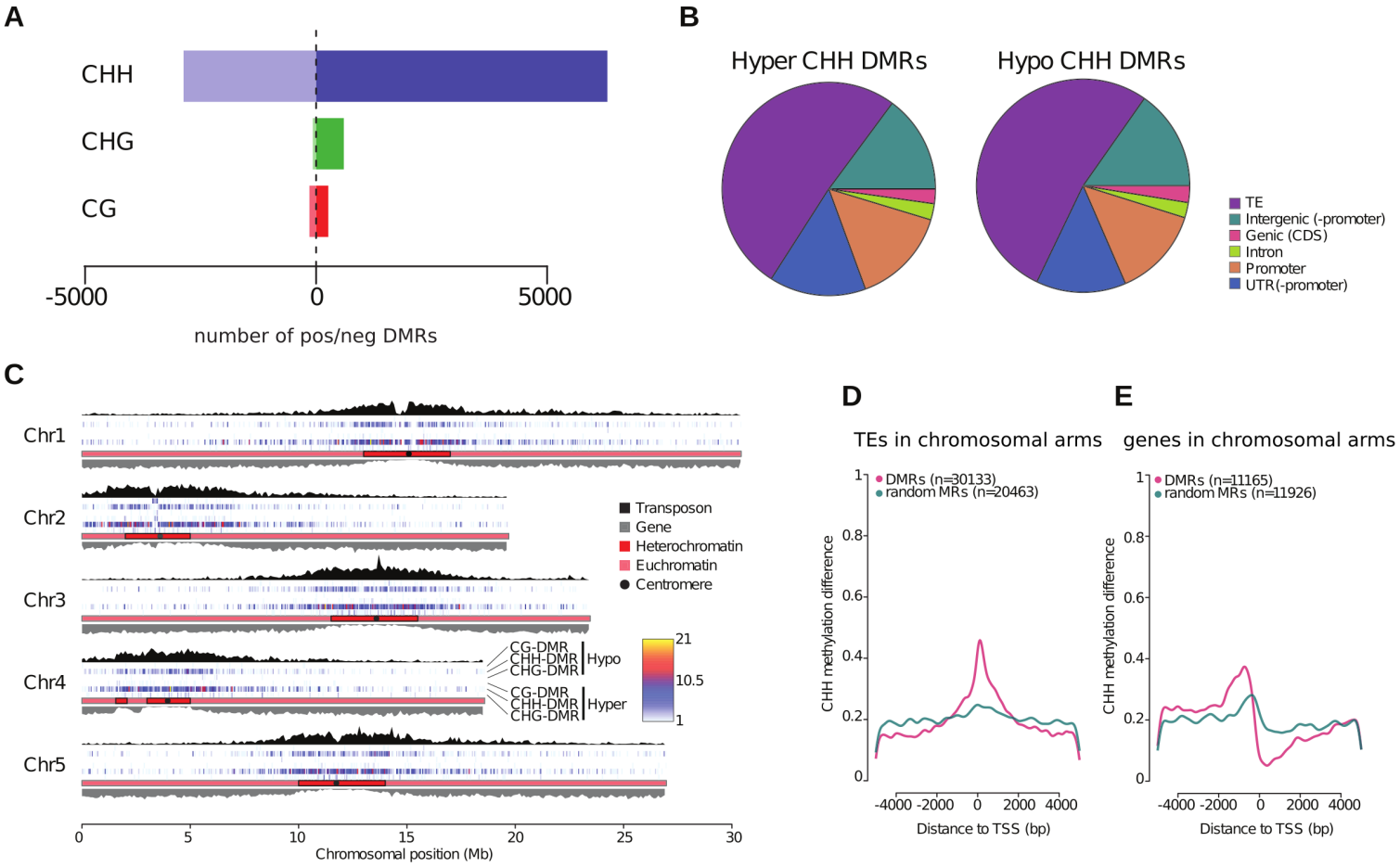

Figure 2
DMRs induced by SylA treatment

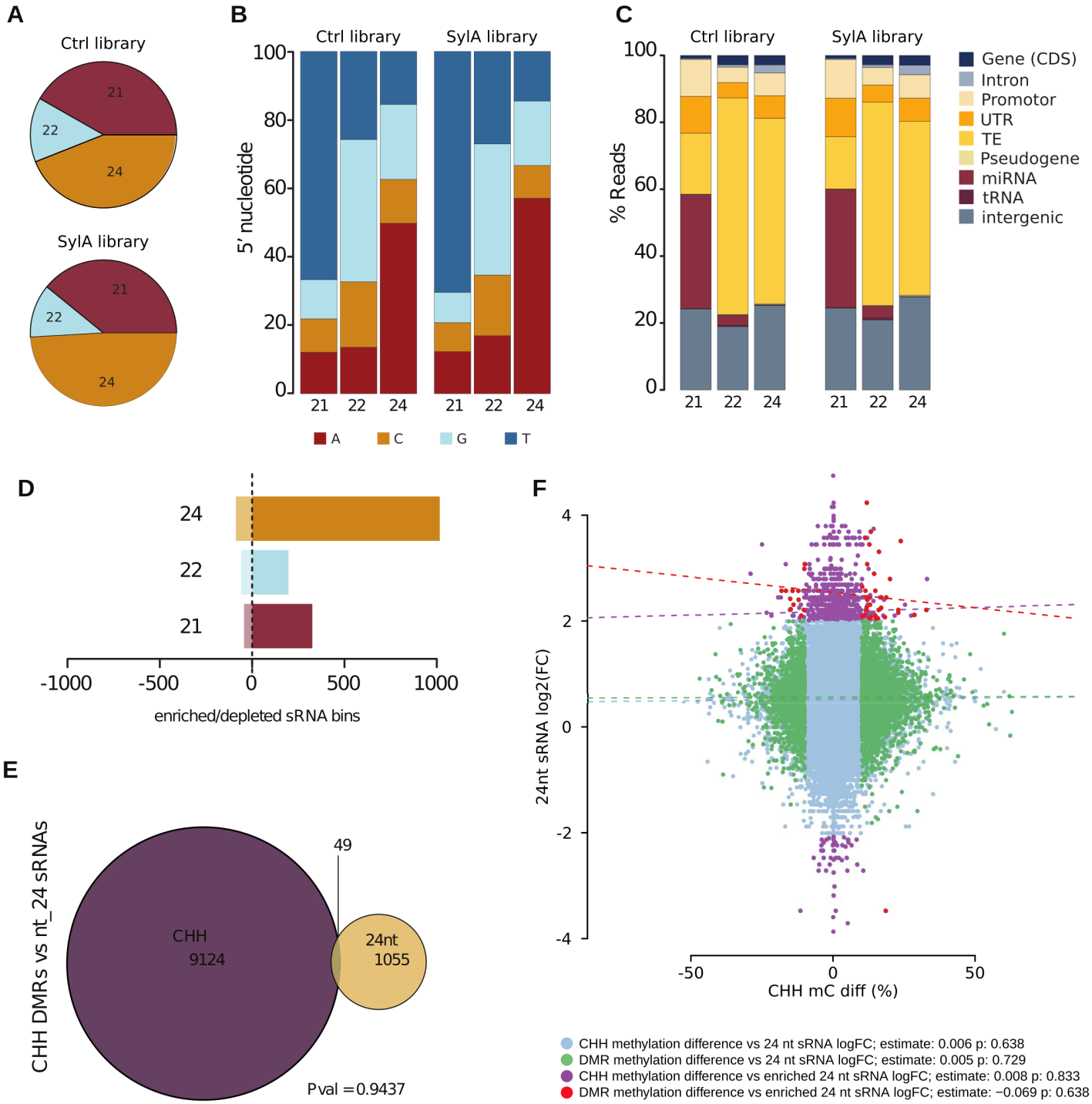

Figure 3
small RNA population upon SyringolinA treatment

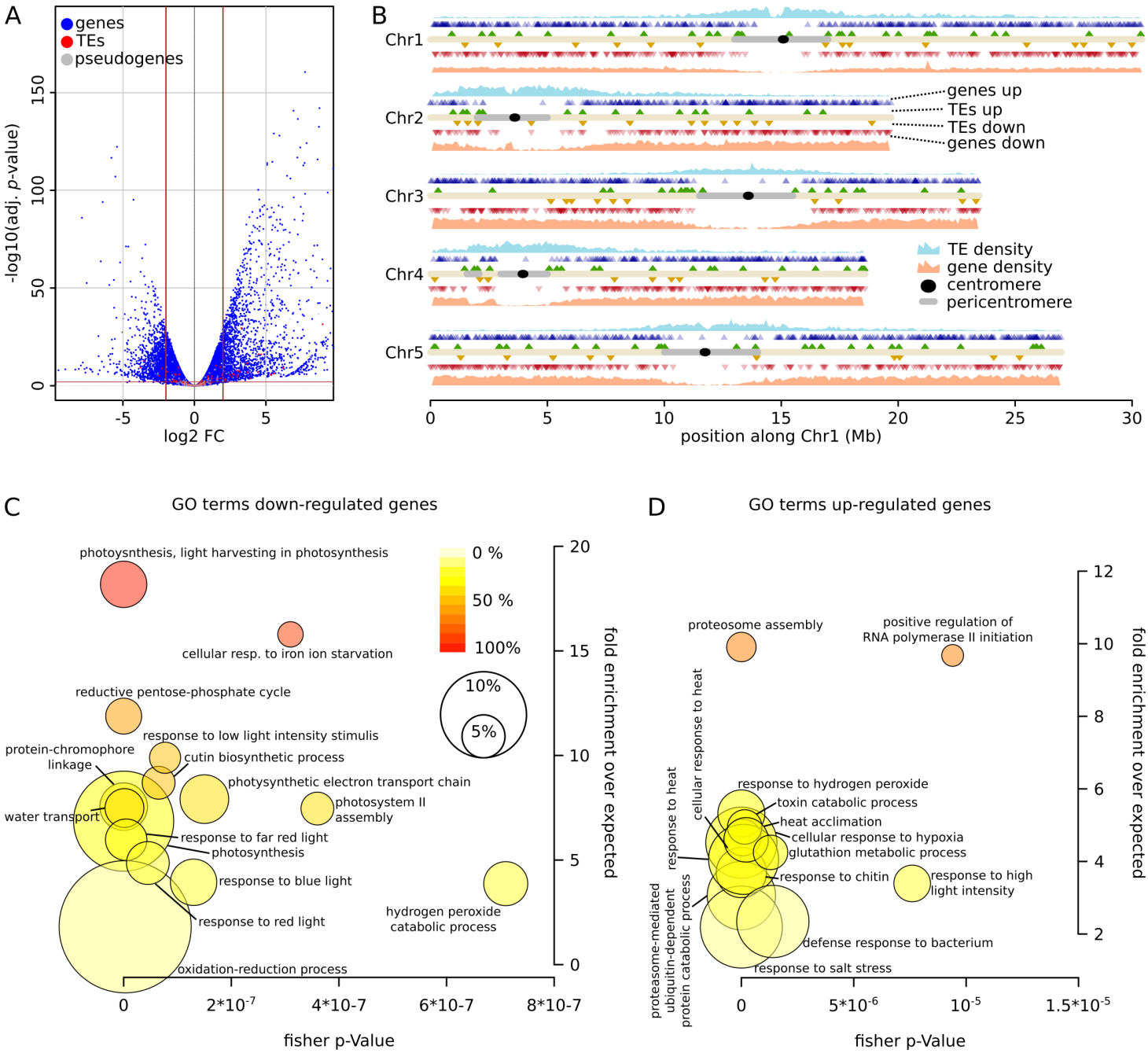

Figure 4.
High number of up-regulated genes upon SylA treatment

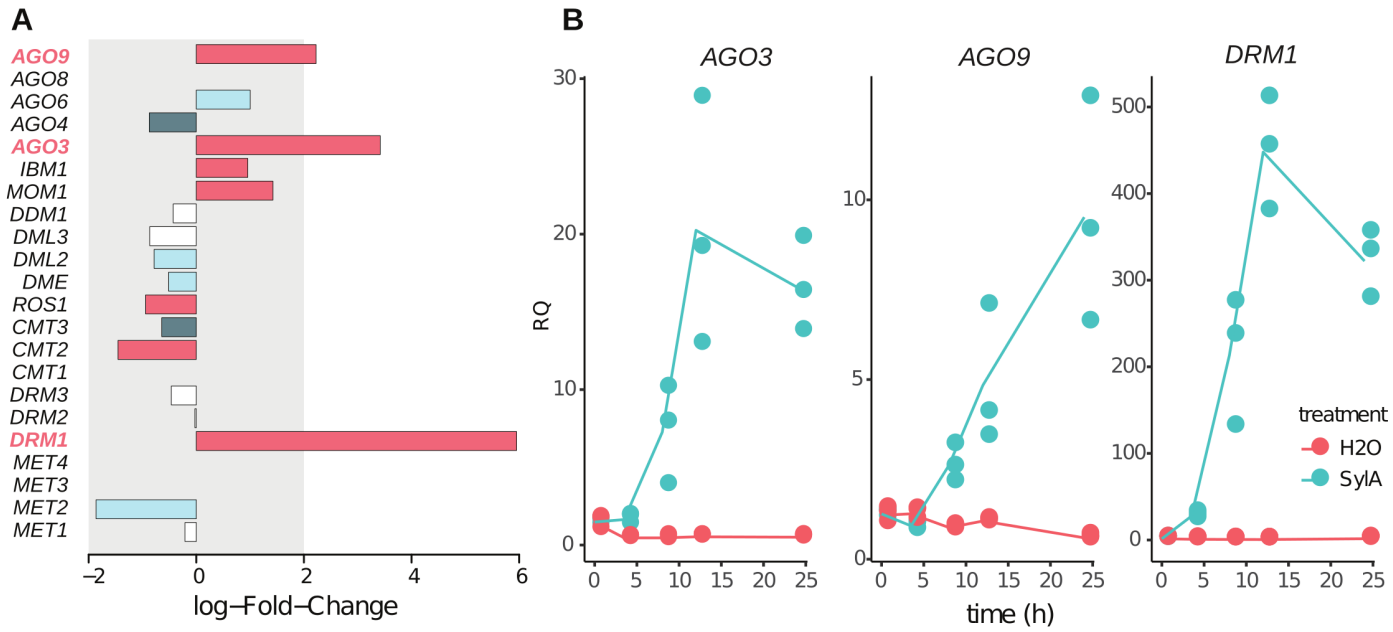

Figure 5.
Syringolin A regulate the expression of AGO3, AGO9 and DRM1

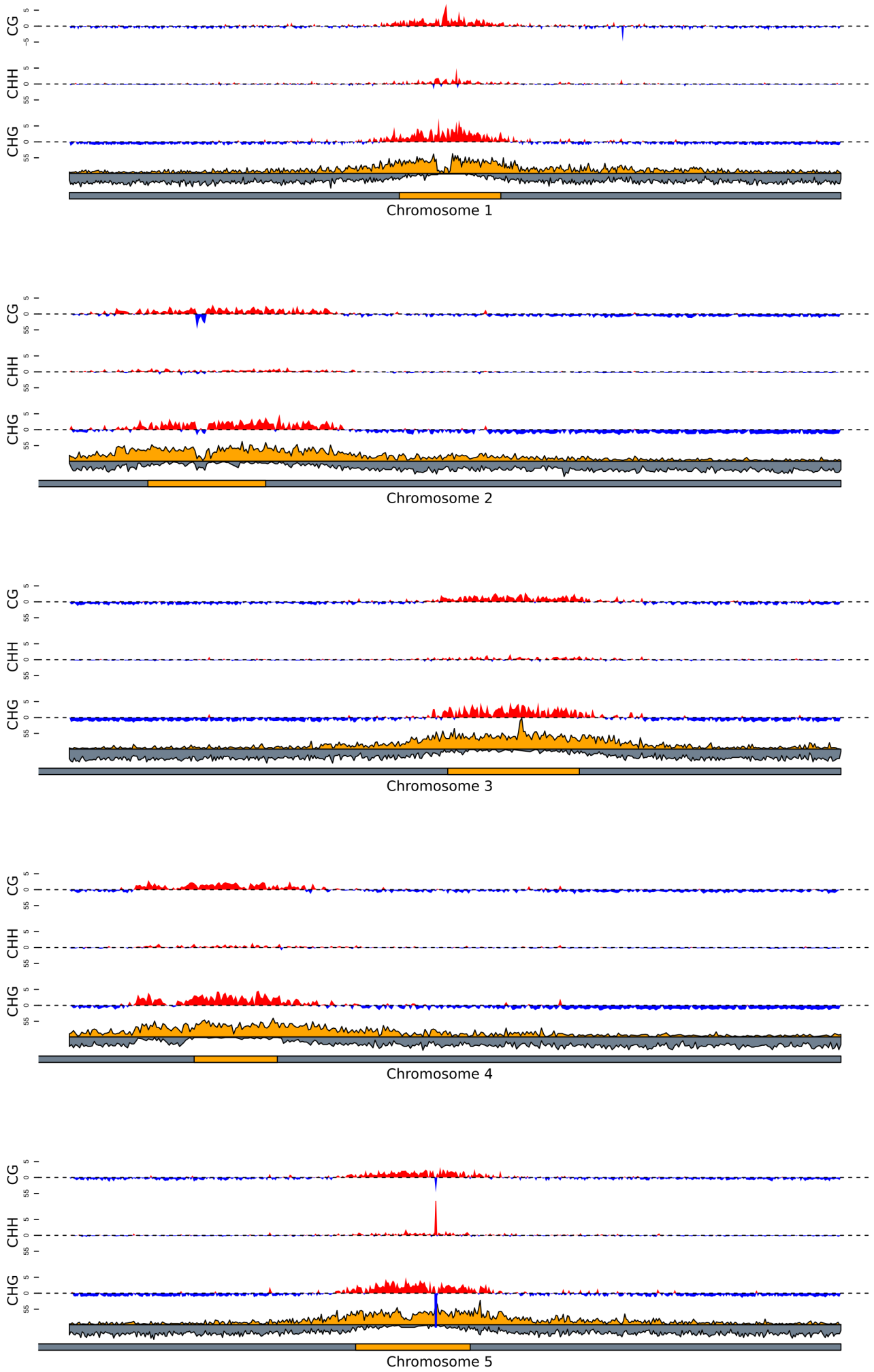

Figure S1
Percent methylation changes along *Arabidopsis* chromosomes

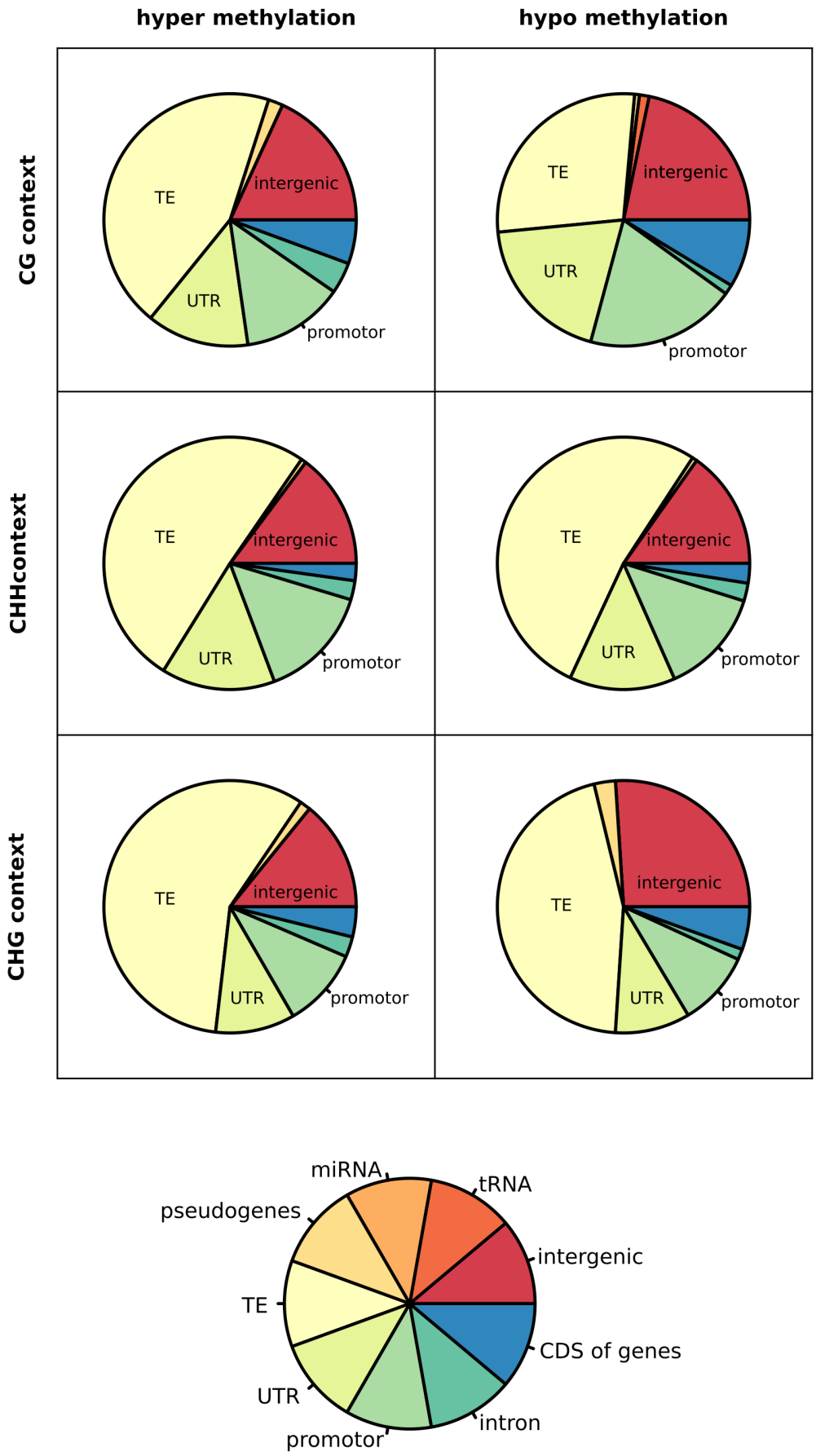

Figure S2
Genomic features associated to DMRs

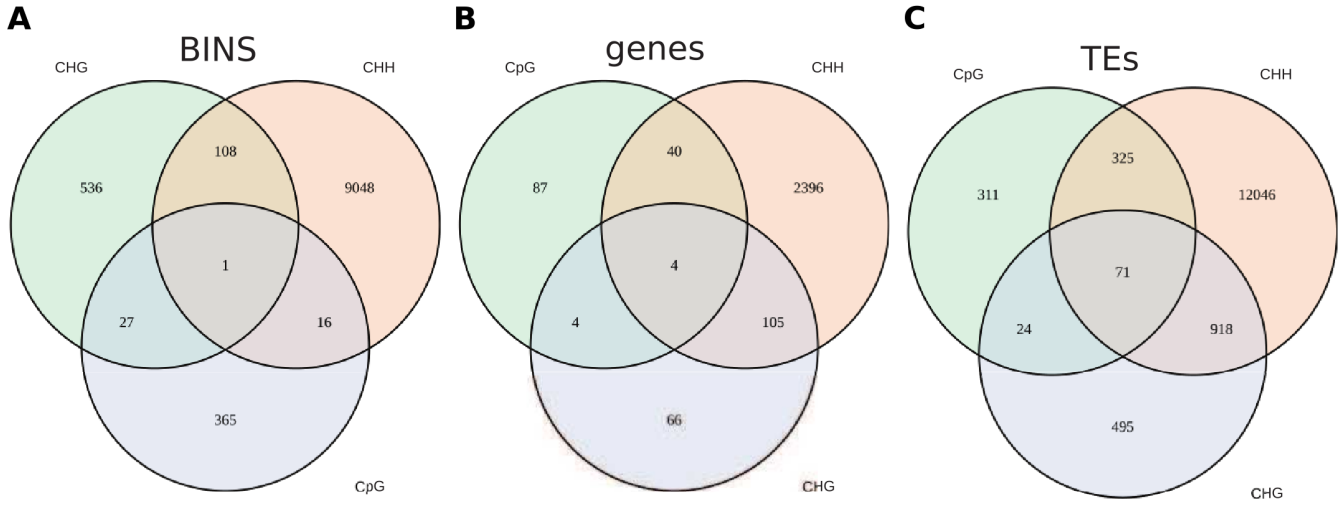

Figure S3
Overlap between DMRs of different sequence contexts

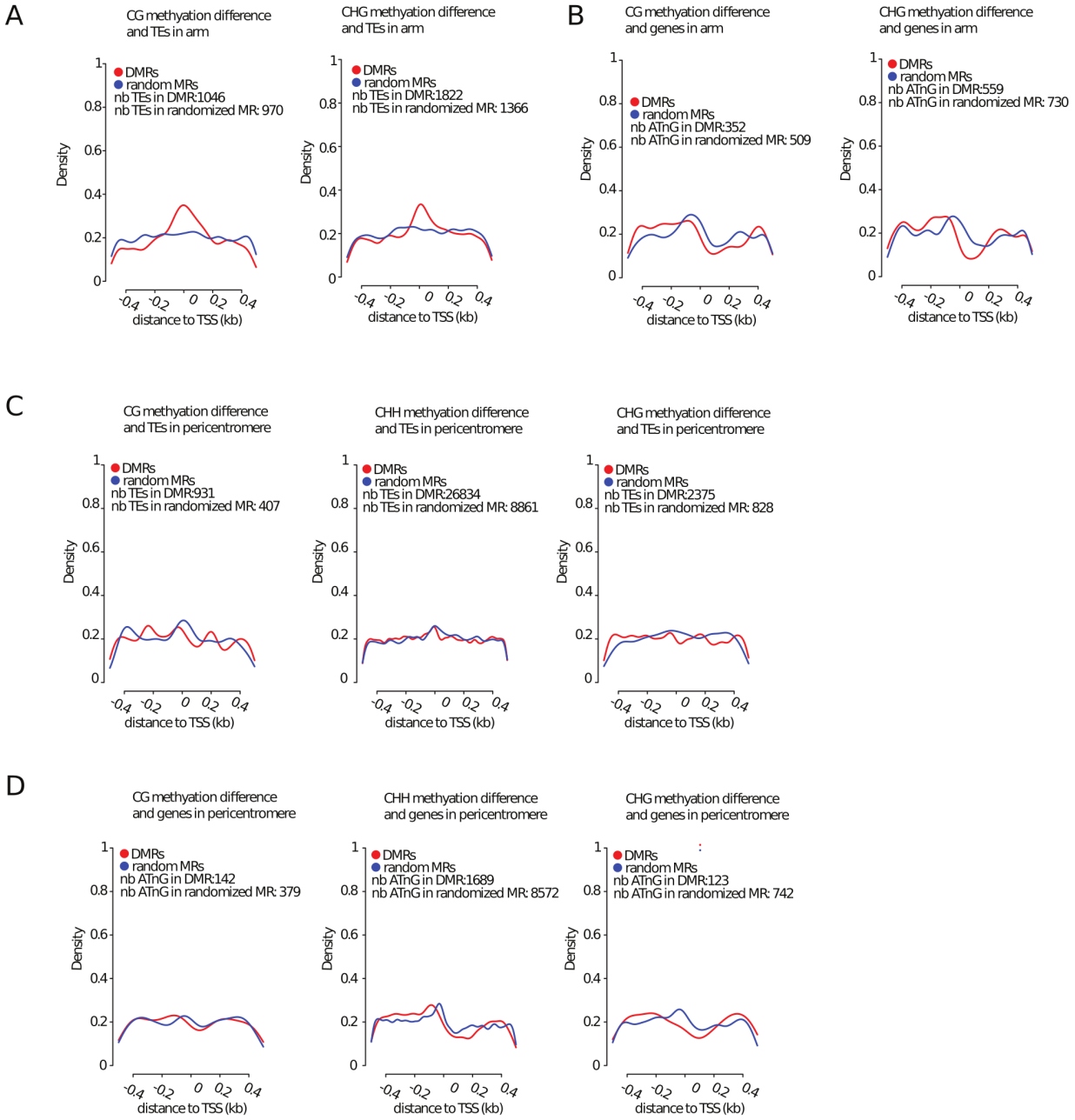

Figure S4
DMRs distance to Transcription start site

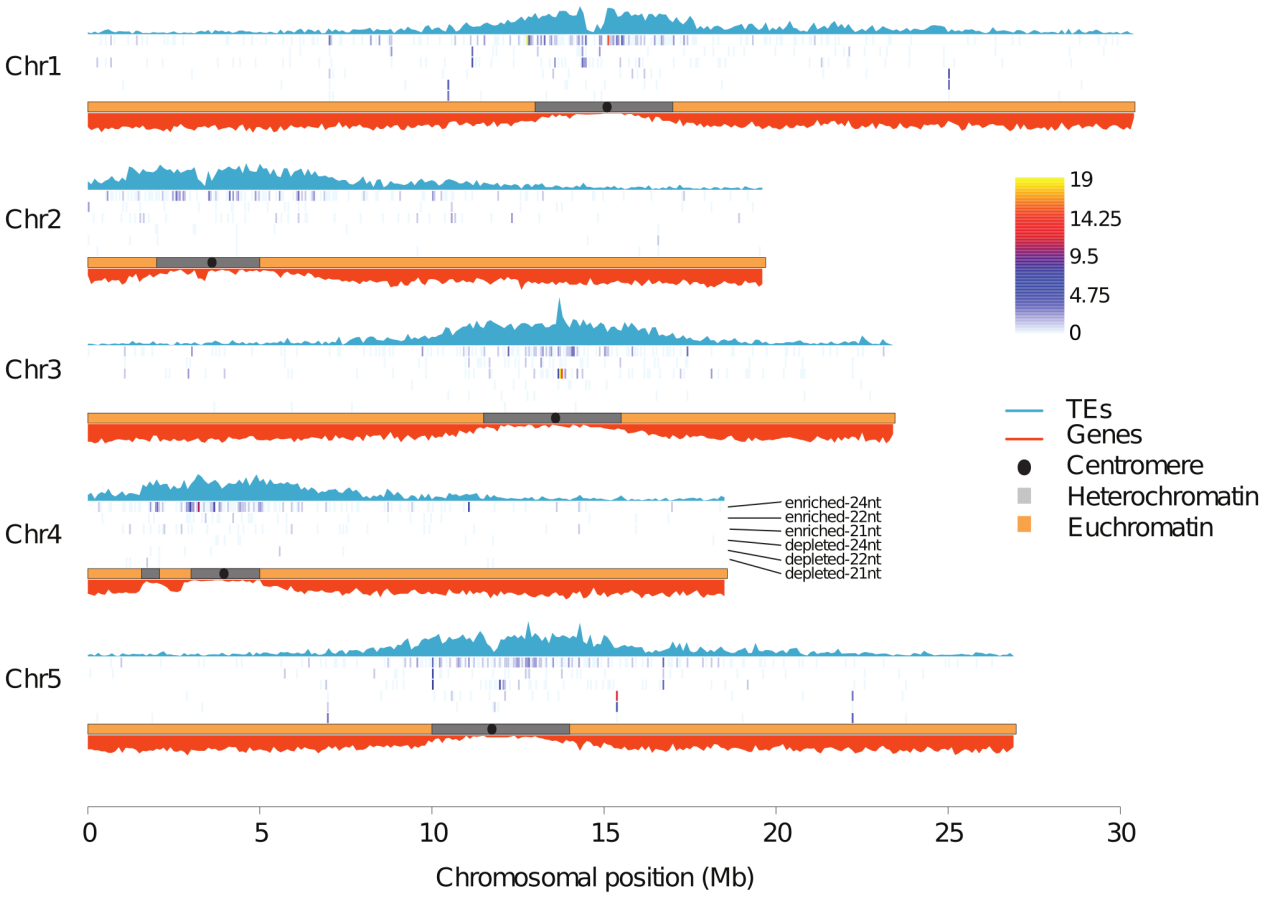

Figure S5
Genomic location of the differencially expressed sRNA bins

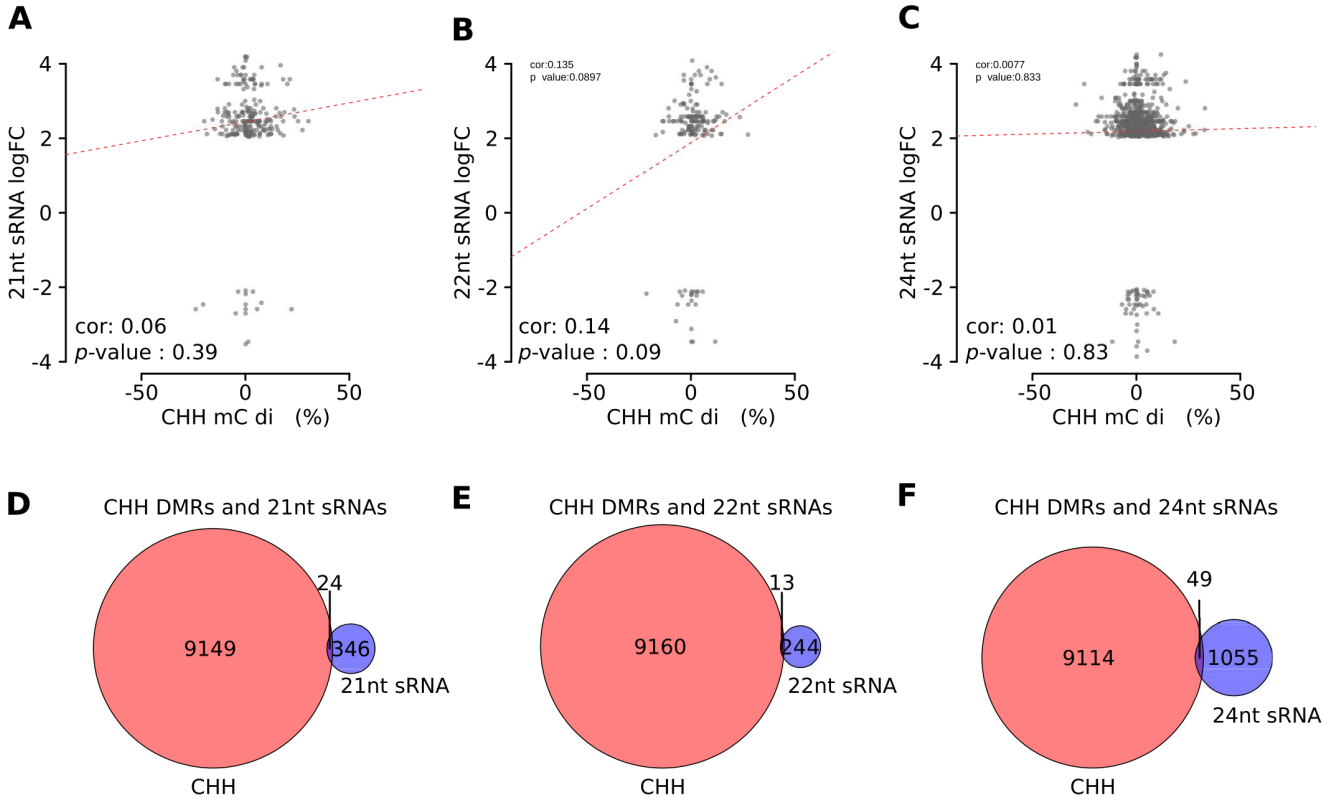

Figure S6
Relationship between differentially expressed sRNA bins and DNA methylation changes

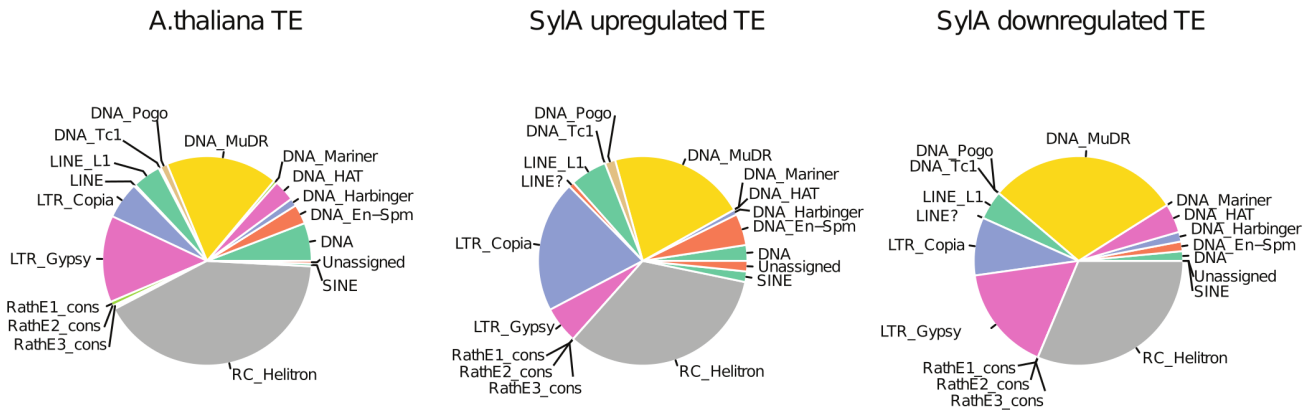

Figure S7
Differentially expressed TE families

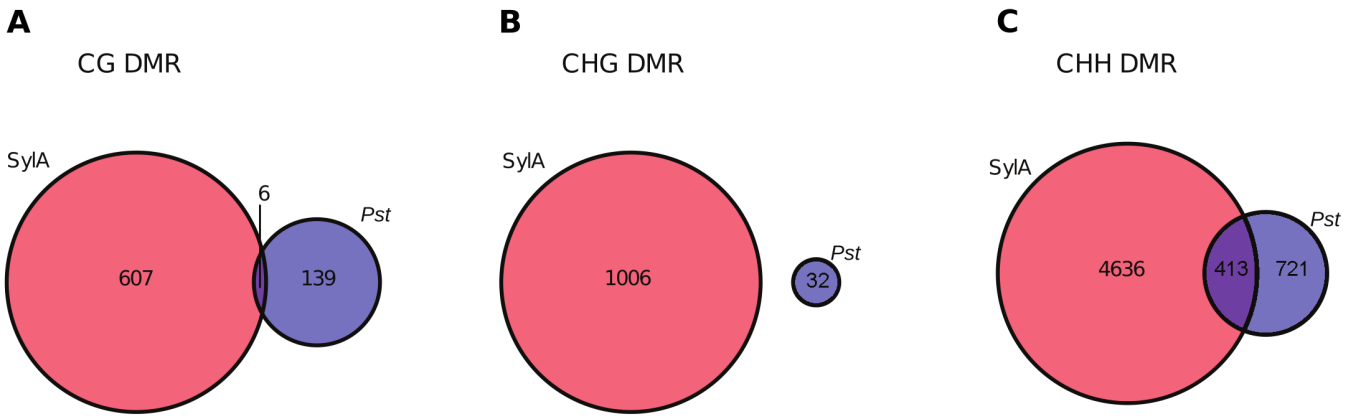

Figure S8

Overlap between SylA and Pst induced DMRs

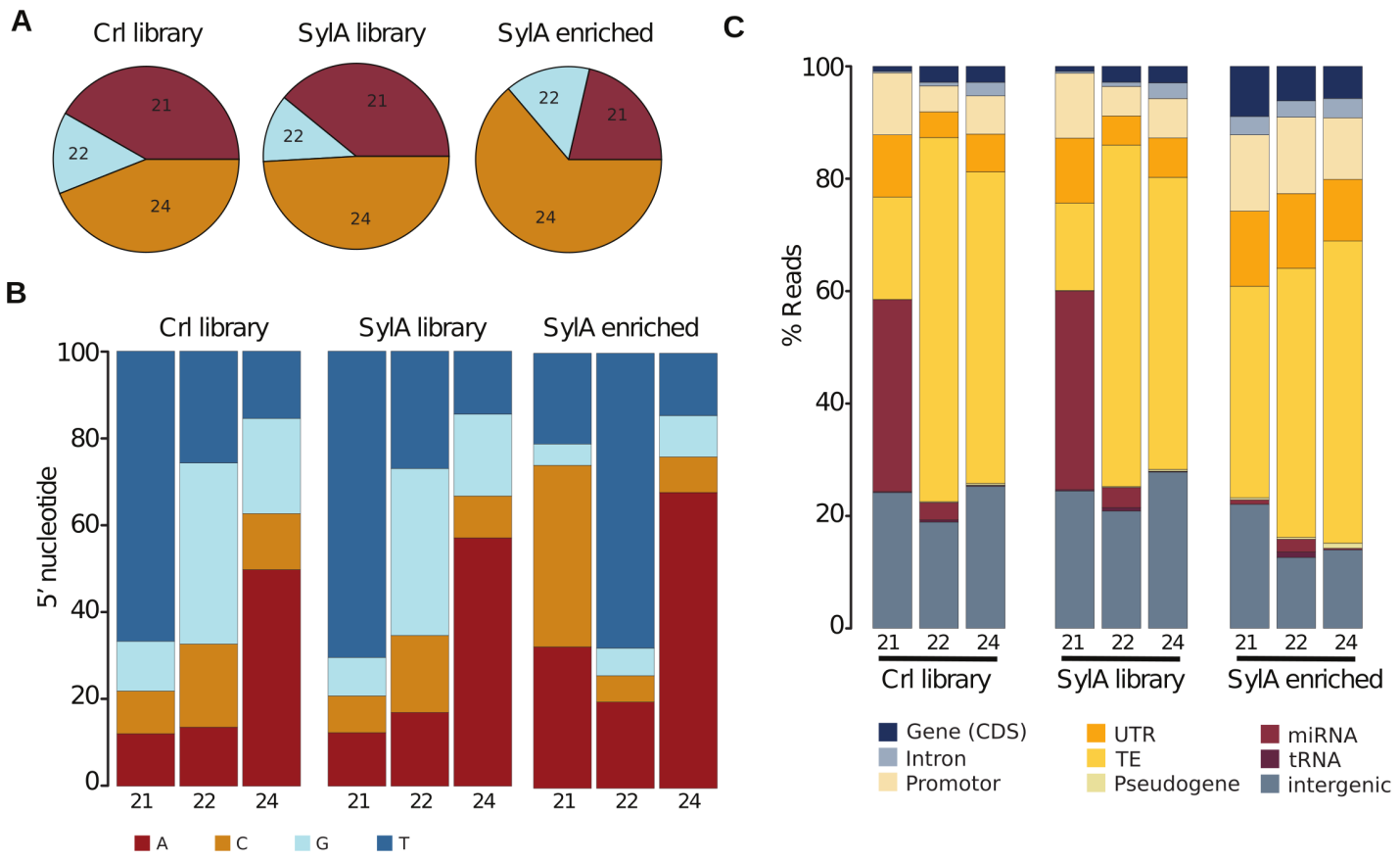

Figure S9

Characteristic of small RNA enriched population upon Syringolin A treatment.